J Comput Neurosci (2013) 35:295–316
DOI 10.1007/s10827-013-0453-9

A single compartment model of pacemaking in dissasociated substantia nigra neurons

Stability and energy analysis

Febe Francis · Míriam R. García · Richard H. Middleton

Received: 13 September 2012 / Revised: 1 April 2013 / Accepted: 3 April 2013 / Published online: 19 May 2013

Abstract Spontaneous oscillations in the mid-brain dopaminergic neurons are an important feature of motor control. The degeneration of these neurons is involved in movement disorders, particularly Parkinson's Disease. Modelling of this activity is an important part of developing an understanding of the pathogenic process. We develop a mathematical paradigm to describe this activity with a single compartment approach and a CellML version is made publicly available. The model explicitly describes the dynamics of the transmembrane potential with changes in the levels of important cations and is consistent with two major observations in the literature regarding its behaviour in the presence of channel blockers. Stability of the model behaviour is determined from the properties of its Monodromy matrix. We also discuss from the perspective of energy, a pharmacological intervention suggested in the treatment of Parkinson's Disease.

Keywords Neuronal pacemaking · Substantia nigra · Energy stress · Parkinson's Disease · Monodromy matrix · Calcium stress

Mathematics Subject Classifications (2010) 92C20 · 92C30 · (70K42)

Action Editor: Charles Wilson

F. Francis · M. R. García (✉)
Hamilton Institute, NUI Maynooth,
Co. Kildare, Ireland
e-mail: Miriam.Garcia@nuim.ie

R. H. Middleton
Centre for Complex Dynamic Systems & Control,
The University of Newcastle,
Newcastle, Australia
e-mail: richard.middleton@newcastle.edu.au

1 Introduction

Oscillatory activities in and among neurons are significant for information processing in the brain. Dopaminergic neurons in the basal ganglia circuit, *substantia nigra pars compacta* (*SNc*), are one of the prominent groups of neurons known for their spontaneous oscillations. These neurons are important for a range of functions including movement related information processing. In Parkinson's Disease (PD), neurons of this group degenerate extensively with consequent pathological motor behaviour.

The autonomous tonic pacemaking of *SNc* neurons is a unique feature that enables motor control. These *SNc* oscillations ensure a continuous supply of dopamine to the striatum, significant for its normal functioning. Also, regular oscillations in *SNc* neurons switch to a bursting mode in response to a stimulus, a behaviour that is associated with spatial learning and temporal processing (Da Cunha et al. 2003; Matell and Meck 2000). Further, these neurons are extensively arborised to provide uniform percolation of dopamine in the striatum (Matsuda et al. 2009).

However, this arrangement comes at a cost. The elaborate arborisation and continuous pacemaking imposes a high energy demand within these neurons. This structural and functional association makes *SNc* one of the most stressed neurons of the brain (Wellstead and Cloutier 2012). Furthermore, these neurons employ calcium ions to establish and maintain their tonic activity (Surmeier 2007). This reliance is conjectured to accelerate normal ageing of these neurons, when subjected to genetic or environmental pressures that supplement the inherent metabolic stress (Wellstead and Cloutier 2011).

It is difficult to comprehend the pathogenic mechanism in idiopathic PD since it is a multi-factorial condition. Contrary to a scenario of single cause and effect, the complexity

presented by the molecular system of *SNc* calls for an integrated framework to model various subsystems contributing to the pathogenesis. For a condition of systemic failure like PD, energy metabolism can be employed as a unifying basis to relate various models depicting events that lead to the disease (Cloutier and Wellstead 2010; Wellstead and Cloutier 2011). In this paper, we attempt to model a subcomponent of the *SNc* machinery, the membrane events contributing to the basal pacemaking activity of these neurons and discuss its energy implications.

All pathways or processes of a living cell are directly or indirectly dependent on its energy metabolism. For an excitatory cell, many of its activities at the membrane are governed by the levels of intracellular ATP and cyclic AMP (cAMP). For instance, ATP has a direct influence on membrane functions via membrane cation pumps. These pumps are 'ATP-ases' and their functioning is critical in establishing electrochemical gradients and resting membrane potential. Transport through ion channels can continue as long as the electrochemical gradient persists. Also, there are certain ion-channels that are ATP sensitive and modulation of these channels, by changes in the level of cytosolic ATP, are reflected in the properties of action potentials produced along the length of the membrane. Thus ATP has an indirect influence on the excitatory properties of these cells and consequently their energy metabolism. On these grounds, ion transport has been argued to be one of the most energy demanding processes in excitatory cells (Attwell and Laughlin 2001).

Neurons are one of the most active cells of an organism and to assure its robustness, the complex architecture of its cellular activities has various components that work towards maintaining system properties. Among the various mechanisms that lend robustness to its signal processing capabilities, are a set of feedbacks between membrane excitation and energy metabolism. As well as energy levels influencing ionic-fluxes, cytosolic ion levels influence ATP production. This interplay is particularly relevant in the case of Ca^{2+} ions. This cation is also taken up by the mitochondria, influencing its membrane potential and modulating the ATP processing capacity (Duchen et al. 2008).

Mathematical models have been extensively used to describe the electrophysiology of *SNc* neurons (Amini et al. 1999; Canavier 1999; Wilson and Callaway 2000; Komendantov et al. 2004; Canavier and Landry 2006; Kuznetsova et al. 2010; Drion et al. 2011). These models have been instrumental in elucidating various components on the *SNc* membrane that work towards establishing its characteristic electrophysiology. An important aspect of the *SNc* pacemaker that these models discuss is how Ca^{2+} ions are significant in establishing this electrophysiology.

L-type calcium channels have a central role in initiating membrane depolarisation that sets the pacemaking cycle (Takada et al. 2001; Chan et al. 2007). Also, the subthreshold oscillations that drive the firing in these neurons are formed from a calcium-potassium mechanism established by a low voltage activation threshold of some of the calcium channels in these neurons (Nedergaard et al. 1993; Surmeier et al. 2005). This calcium driven mechanism of membrane oscillations has been reported to be present in all parts of this neuron (Wilson and Callaway 2000), strongly coupled with membrane voltage.

Chan et al. (2007) demonstrates how neurons of *SNc* are capable of re-establishing pacemaking when their calcium channels are blocked, with the help of Na^+ ions. This is based on an observation that juvenile neurons starts off their characteristic pacemaking driven by Na^+ currents. As they age, with higher expression of L-type calcium channels, this dependence is replaced by an efficient Ca^{2+} driven mode. When L-type calcium channels are blocked, with a little increase in cytosolic cAMP concentrations, Chan et al. (2007) were able to shift the voltage dependence of HCN channels to initiate and resume pacemaking. Later, it was demonstrated that the L-type calcium channels are not really essential for these neurons to function and this has been a point of controversy with a suggested use of L-type channel blockers as a preventive therapy in PD (Surmeier 2007).

For a cell that relies heavily on Ca^{2+}, the disposition of these ions become decisive. One of the major findings with respect to PD pathogenesis, is related to the calcium handling aspects of *SNc* neuron. It was reported that neurons that express higher levels of calbindin, a calcium binding protein, are relatively spared from degeneration (Damier et al. 1999). This study strongly suggests a pivotal role of calcium stress in the neurodegenerative process and for this reason, mechanisms involved in Ca^{2+} disposal needs to be considered in models that aim to relate pathways leading to the degeneration of these neurons.

Although, some of the mathematical models previously presented do incorporate mechanisms for Ca^{2+} buffering (Wilson and Callaway 2000) or removal by a calcium pump (Amini et al. 1999), most often these steps are abstract, or at best simplified models are used with little attention to the dynamics of the Ca^{2+} pumps and/or buffers. These limitations are potentially serious in any study of Ca^{2+} mechanisms in the electrophysiology and functioning of these neurons.

SNc neurons have been observed to be capable of spontaneous oscillation even when they are acutely dissociated (Puopolo et al. 2007). This suggests that the *SNc* perikaryon contains the basic machinery required for its spontaneous firing and that dendritic inputs are not really essential in initiating pacemaking. This observation suggests the possibility of understanding and analysing the underlying mechanism of oscillation, without considering the network of dendrites that constitute this neuron. Such an

approach can also help in identifying some of the attributes of its membrane electrophysiology that makes them vulnerable to degeneration in PD, without the need for a complex coupled model. Based on this concept we have designed our model based on a geometry that we would be referred to as 'the pacemaking unit' (PMU).

In this paper we propose an approach to mathematically modelling the electrophysiology of *SNc* neurons that is a little different from the usual ones. To begin with, we explicitly describe the dynamics for the transmembrane potential in terms of ionic concentrations. Next, owing to significant differences in the ion dynamics inside the cell, we prefer to use an electrodiffusion model for channel conduction compared to the commonly used linear conductance relationship. This is particularly important in the case of Ca^{2+} ions due to the large driving force of transport that exist for these ions across the membrane. Also, we use Markov models for the ionic pumps to incorporate the nuances of the limiting steps that control the dynamics of these proteins. Although, these changes have been attempted previously (Francis et al. 2012a, b), some key geometric features were idealised, and not representative of a real *SNc* neuron.

Global optimisation strategies were used to identify important parameters of the model. The resulting model was validated for expected behaviours for a set of perturbations. The model was also mathematically inspected for the presence of stable limit cycles by numerically computing the Monodromy matrix of the linearisation about the limit cycle. Finally, the model is used to investigate the cost of pacemaking in terms of energy expenditure as a function of ATP usage.

The model presented in this article may be later incorporated into a larger framework of energy metabolism in *SNc* neurons. Towards this end, our pacemaking model has been translated into CellML, and the model is freely available for download from http://models.cellml.org/e/12b. CellML is an open standard XML-based markup language used for developing and sharing mathematical models of biological processes (Lloyd et al. 2004, 2008).

2 Model description

To both understand pacemaking of *SNc* neurons and estimate energy requirements for this process, in both normal conditions and under L-type channel blockers, we develop a model of ordinary differential equations including membrane voltage, relevant ionic concentrations, ion channel gatings and calcium buffers. In the following subsections we describe the main components for *SNc* pacemaking and the considered cell morphology. First, we focus on the membrane dynamics, intracellular buffering and the estimation of energy required.

2.1 Selection of components for *SNc* pacemaking

One of the biggest challenges in the development of electrophysiological models is the identification of important types of channel proteins that contribute to the typical response of the neuron. Traditionally this is understood from studies involving channel blockers, but the resolving power of these experiments is not always good. The analysis can sometimes be limited for a variety of reasons, including problems with experimental design and set up, non-specificity of the blocker molecule towards a range of channel proteins, variability in the expression levels of target proteins in the region of interest etc.

In order to have a reasonable understanding of key elements at the membrane, involved in the characteristic signalling of these neurons, we examined data on the protein expression profiles for cation channels from the datasets of Moran et al. (2006) and Lesnick et al. (2007). Table 1 gives a comprehensive list of different cation channels expressed by these neurons.

Although it is possible to model and connect all the different channels that are apparently expressed in a neuron, there are problems with this approach. The first difficulty is that this would result in a complex model with large number of components, which in turn would make the model less comprehensible and appropriate for analysis. Secondly, a large number of parameters would likely result in identifiability problems. In such cases, despite being able to reproduce the experiments used for calibration, there are whole families of parameter values that also reproduce the data, and therefore have no physical meaning and in turn make the model limited in its predictive capabilities (Balsa-Canto et al. 2010).

A further important limitation of overly complex models is the difficulty in determining the electrophysiological characteristics of the large number of ion-channels involved. Frequently, such characteristics are adapted from experiments that are not necessarily conducted with the same organism for which the larger model is developed (for example see Amini et al. (1999)). Even though these proteins are functionally conserved among species, there are species to species differences in their post translational processing and variations in the choice of sub-units for their quaternary structure. Such differences, though subtle, are reflected in the dynamic response of these channels. Further, experiments on ion-channels are frequently conducted in conditions that are different from their native physiological environment. Parameters identified from such experiments when used in larger models, may lead to skewed interpretations of the phenomenon. On these grounds, mathematical models of neurons are necessarily simplifications that may represent some observable aspects of neuronal behaviour, but

Table 1 *SNc* cation channels

Channel	Type	Gene symbol
Voltage-gated Ca^{2+} channel	L-type	CACNA1C ($Ca_v1.2$), CACNA1D ($Ca_v1.3$)
	T-type	CACNA1G ($Ca_v3.1$), CACNA1I ($Ca_v3.3$)
	P/Q - type	CACNA1A ($Ca_v2.1$)
	N - type	CACNA1B ($Ca_v2.2$)
Voltage-gated Na^+ channel		SCN1A ($Na_v1.1$), SCN2A ($Na_v1.2$), SCN3A ($Na_v1.3$), SCN9A ($Na_v1.7$), SCN11A ($Na_v1.9$)
Voltage-gated K^+ channel	Delayed rectifier	KCNA1 ($K_v1.1$), KCNA6 ($K_v1.6$), KCNB1 ($K_v2.1$), KCNC1 ($K_v3.1$)
	A-type	KCNC4 ($K_v3.4$), KCND2 ($K_v4.2$), KCND3 ($K_v4.3$)
	Inward-rectifying	KCNH2 ($K_v11.1$), KCNH7 ($K_v11.3$)
	Slowly - activating	KCNH8 ($K_v12.1$)
Inward-rectifying K^+ channel	Voltage gated	KCNJ2($K_{ir}2.1$), KCNJ10 ($K_{ir}4.1$), KCNJ14 ($K_{ir}2.4$)
	G protein-coupled	KCNJ6 ($K_{ir}3.2$), KCNJ9 ($K_{ir}3.3$)
Calcium-activated K^+ channel	BK	KCNMA1 ($K_{Ca}1.1$)
	SK	KCNN2 ($K_{Ca}2.2$), KCNN3 ($K_{Ca}2.3$), KCNT2 ($K_{Ca}4.2$)
Leak channel		NALCN (mostly responsible for sodium leak)
Tandem pore domain K^+ channel		KCNK1 ($K_{2p}1.1$), KCNK10 ($K_{2p}10.1$), KCNK12 ($K_{2p}12.1$), KCNK17 ($K_{2p}17.1$)
Hyperpolarization-activated cyclic nucleotide gated channel	HCN	HCN1, HCN2, HCN4
Two pore segment channel		TPCN1, TPCN2

A list of cation channel α sub-units expressed in Human substantia nigra based on the datasets of Moran et al. (2006) and Lesnick et al. (2007). Channels that are underlined are later used in the model

where many lower level details are treated in a simplified manner.

For these reasons, we focus on ion-channels that have been reported to contribute to pacemaking (Amini et al. 1999; Wilson and Callaway 2000; Puopolo et al. 2007; Kuznetsova et al. 2010). L-type calcium channels and sodium channels are both significant in driving the pacemaker activity of these neurons (Putzier et al. 2009; Drion et al. 2011) and the fast sodium along with delayed rectifier potassium currents function towards generating spikes (Amini et al. 1999). Small conductance (SK)—calcium gated potassium channels are understood to be crucial in establishing underlying slow wave oscillations and the stability of spontaneous pacemaker activity (Wolfart and Roeper 2002; Ibanez-Sandoval et al. 2007). The characteristic of inward rectification is realized by a representation for an internally rectifying potassium channel and a leak current based on sodium is also included.

The balancing act of the ion-transport is assigned to the activities of the sodium-calcium exchanger (NaCax), plasma membrane calcium ATP-ase (PMCA) and the sodium-potassium ATP-ase (NaK). Because of its important as a signalling molecule, Ca^{2+} levels in cells have to be kept strictly regulated. To a large extent buffering mechanisms in the cell account for the restraint in Ca^{2+}. The machinery involved in this activity involves mobile Ca^{2+} sequestering proteins as well as organelles that store Ca^{2+}, like the endoplasmic reticulum and mitochondria. A detailed description of intracellular calcium dynamics is out of the scope of this article, as we aim to focus at events in the vicinity of the plasma membrane contributing to the pacemaking in these neurons. For this reason, we incorporate the dynamics of only two mobile Ca^{2+} buffers, that are fast and often found localized at calcium hotspots adjacent to the plasma membrane. Further, these proteins, calbindin and calmodulin have been implied in PD pathogenesis (Yamada et al. 1990; Zhou et al. 2010; Iwatsubo et al. 1991).

2.2 Cell morphology

The electrical characteristic of a neuron is essentially a membrane phenomena and for this reason, morphological features that define the neuron have a significant role in the realization of its electrophysiology. For a neuron like *SNc* that is highly arborized, defining a model geometry that is anatomically realistic is a challenge. Additionally, it is difficult to translate an exact spatial distribution of ion-channels across the membrane landscape. However, *SNc*

neurons exhibits regular pacemaking even when acutely dissociated (Hainsworth et al. 1991; Puopolo et al. 2007) and this feature offers a way of establishing a geometry for modelling these neurons without including its extensive dendritic efferents.

We define a pacemaking unit (PMU), that models the *SNc* soma and immediate dendritic regions that radiate from the soma. This is modelled in a way that includes a region like the axon hillock, that has a high density of ion-channels responsible for the characteristic electrophysiology of this neuron. Based on various micrographs observed in literature (Matsuda et al. 2009; Puopolo et al. 2007; Tepper 2010), the unit is assumed to be best represented by a hyperbolic tetrahedron (see Fig. 1), with a large surface-to-volume ratio than regular geometries that are usually used such as spheres and cylinders. This unit is a part of an acutely dissociated *SNc* neuron, capable of spontaneous pacemaking. For the model, we consider constant ionic concentrations in the extracellular space and assume the PMU to be in an osmotic equilibrium with its environment, so that cell dimensions are preserved in the course of the process. The parameters for this geometry are provided in Table 2.

2.3 Membrane dynamics using the conservation principle

Most efforts to model neuronal pacemaking use the modelling paradigm established by Hodgkin and Huxley (1952) to calculate the membrane potential. In its original form which we would address here as the 'differential form', the transmembrane potential (V) is determined from a differential equation defined by the net current flowing through ion-channels on the membrane, based on Kirchoff's law.

$$\frac{d(V)}{dt} = \frac{1}{C_m} \sum_{x \in X_s} I_x \tag{1}$$

Here C_m is the membrane capacitance and $s \in S = \{Na, Ca, K, A\}$ represents sodium, calcium, potassium and anions respectively, that are crucial in establishing the membrane potential. Such models do not necessarily satisfy the conservation principle of ionic species and are the only alternative when the dynamics of cytosolic concentrations of contributing ions are not included in the model. Later models of excitable cells include the dynamic changes associated with intracellular cations (for example, DiFrancesco and Noble (1985)), often in an implicit manner. However, such models are often criticized for their behaviour under prolonged simulations, including drifts of ion concentrations, membrane potential as well as existence of multiple steady states (Hund et al. 2001).

As an alternative, "algebraic" models have been suggested to account for such problems (Endresen et al. 2000; Poignard et al. 2011), to give a paradigm that is stable with respect to the drift in computed variables. The algebraic equation is typically an integrated version of the differential form of the voltage expression and formulated using ionic charge conservation principles (Varghese and Boland 2002). For cells whose shapes are retained by an osmotic equilibrium (Poignard et al. 2011), we can represent this as

$$V = \frac{F \mathcal{V}_{cyt}}{C_m} \sum_{s \in S} z_s [s_i - s_e]. \tag{2}$$

Here F represents the Faraday constant, $\mathcal{V}_{cyt}$ the cytosolic volume, and z_s the valency of ionic species s with s_i and s_e denoting the intracellular and extracellular concentrations, respectively. Considering the fact that ionic concentrations in the extracellular space and intracellular anions do not present significant variations (Endresen et al. 2000), the membrane potential is essentially a function of changes in intracellular cation concentrations.

Hund et al. (2001) suggests that if charges are conserved, the choice of method (differential or algebraic) does not influence the behaviour of the system. In the case of using the algebraic form, we need to be cautious with the choice of initial conditions and the integration constant, as the model tends to be sensitive to this choice particularly during numerical simulation. Although the differential form has an additional state variable, we adopt this norm for our model

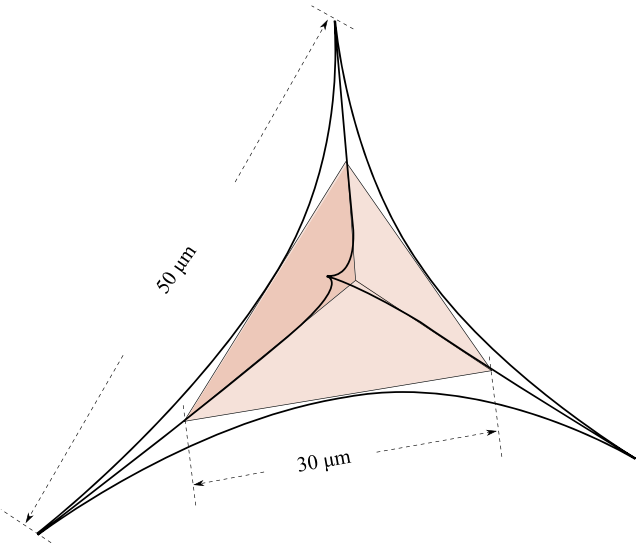

Fig. 1 Morphology considered: a pacemaking unit (PMU), which mostly comprised of the *SNc* soma and immediate dendritic regions that radiate out from the soma including axon hillock. The neuronal soma is considered to be a tetrahedron with a dimension not more than 30 μ as observed in anatomical studies (Grace and Bunney 1983). The soma extends to form the major dendrites such that the entire PMU assumes the shape of a hyperbolic tetrahedron

Table 2 Model parameters: geometry

Item	Symbol	Value (Units)	Reference
Characteristic dimension, soma	d_s	30 (μm)	Matsuda et al. (2009)
Characteristic dimension, PMU	d_{pmu}	50 (μm)	Tepper (2010)
Volume, PMU	$\mathcal{V}_{pmu}$	5 (pl)	approximated
Surface area-to-volume ratio, PMU $\left(\frac{\mathcal{A}_{pmu}}{\mathcal{V}_{pmu}}\right)$	$\mathcal{S}_{pmu}$	16.667(μm^{-1})	fitted
Volume fraction, Cytosol	ϕ_{cyt}	0.5	Alberts et al. (2002)

and formulate it by explicitly relating the transmembrane potential to the dynamics of intracellular concentrations, as

$$\frac{d(V)}{dt} = \frac{F\mathcal{V}_{cyt}}{C_m}\sum_{s\in S} z_s \frac{d(s_i)}{dt} \tag{3}$$

Within the neuron, various cellular mechanisms work towards establishing a dynamic equilibrium for the different ionic species. The most pronounced of them is the concerted engagement of various membrane proteins including ion-channels, exchangers and pumps. Whereas these activities are enough to represent the main dynamics for sodium and potassium, the case with calcium is different. Calcium is an important second messenger implied in downstream signalling and intracellular sequestering mechanisms that help establish its basal levels become relevant.

The dynamics of intracellular ionic concentration depend therefore on membrane currents across the membrane and sequestering mechanisms for calcium, collected in X_s and Y_{ca2+} respectively. Considering mass conservation, the accumulation of intracellular ions for a species "s" can be formulated as Ermentrout and Terman (2010):

$$\frac{d(s)}{dt} = \frac{1}{z_s F\mathcal{V}_{cyt}}\sum_{x\in X_s} I_x + \sum_{y\in Y_{ca}2+} J_y \tag{4}$$

where I_x represents the ionic current through membrane proteins, both channels and transporters and J_y the buffering reactions.

2.3.1 Transport through ion-channels

The transport of ions across the membrane through ion-channels may generalized as

$$I_{s,c} = \mathcal{O}_c(V, s_i, s_e) f_{s,c}(V, s_i, s_e) \tag{5}$$

where the sub index c states for the different ion channels to be considered. Here, f_s is a function that defines the transport influenced by the given electrochemical field and $\mathcal{O}_c$ represents the channel gating or probability of channel c being open. This gating depends always on the membrane potential and, in some cases, also on some ionic concentrations.

We will described here the generalities and the reader is referred to Appendix A 1-4 and Table 4 for more details about the different ion channel models.

Electrochemical transport In the model, we will use two different functions for this transport. On the one hand, using Ohm's law we obtain the usual expression used by Hodgkin and Huxley (1952), linear with respect to voltage:

$$f_{s,c} = \mathcal{G}_{s,c}(V - \bar{V}_s) \tag{6}$$

with $\mathcal{G}$ being the maximal channel conductance according to the linear relationship. $\bar{V}_s$ represents the Nernst potential, the equilibrium condition at which the net transport of the species across the membrane is zero:

$$\bar{V}_s = \frac{V_\tau}{z_s}\ln\frac{s_e}{s_i}, \quad s \in S. \tag{7}$$

Here, $V_\tau = \frac{RT}{F}$ is a temperature defined thermodynamic entity, R is the gas constant and T the physiological temperature.

On the other hand, the electrodiffusion model for channel conduction developed by Hodgkin and Katz (1949), may be expressed using hyperbolic functions to obtain the modified form of Goldman-Hodgkin-Katz (GHK) equation (Endresen et al. 2000)

$$f_{s,c} = g_{s,c}\sqrt{s_e s_i}\frac{sinh\left(z_s\frac{V-\bar{V}_s}{2V_\tau}\right)}{sinhc\left(z_s\frac{V}{2V_\tau}\right)}. \tag{8}$$

Here, the cardinal hyperbolic function $sinhc$, is given by $sinhc(x) = sinh(x)/(x)$.

Many mathematical models in the literature use the linear conductance model of ion-channels and the differential form of the voltage equation with constant intracellular ionic species. The electrodiffusion model (Eq. 8) is mostly used in situations when there are significant differences in the ion dynamics inside the cell, typically with calcium ions. The elaborate description of intracellular ion dynamics and charge conservation, calls for the calculation of such variations. Our model employs the modified form of the GHK (Eq. 8) in most cases. The exception to this is for channels where we have not been able to find suitable clamp data reported in the literature, and therefore for a small number

of channels, we have adopted gating characteristics directly from the literature.

Channel gating We have used three different ways of describing the opening of ion-channels. In the first group, we have channels whose voltage dependent gating are described with the popular Hodgkin-Huxley formalism (Hodgkin and Huxley 1952). According to this formulation, the channel opening probability ($\mathcal{O}$), is a function of channel gates that may activate the channels or inactivate them. Thus,

$$\mathcal{O}_c(V) = [m_c(V)]^{a_c}[h_c(V)]^{b_c} \tag{9}$$

where for channel c, a_c and b_c are respectively the numbers and m_c and h_c the fraction of activation and inactivation components in the conductive state. A first-order differential equation is used to describe the dynamics of each of the gating variables

$$\frac{d(y)}{dt} = \frac{y_\infty - y}{\tau_y}, \quad y \in \{m_c, h_c\}. \tag{10}$$

A Boltzmann-type equation best describes the steady state values of these variables (y_∞) and the time constant (τ_y) is mostly described by an empirical expression which is often a Gaussian function (Izhikevich 2007).

In the second group, we have the channel gating expressed as a simple Markov transition between two states of each individual gates. Here we have,

$$\mathcal{O}_c = \mathcal{O}_1(V)\mathcal{O}_2(V), ..., \mathcal{O}_{n_c}(V) \tag{11}$$

$$\frac{d(\mathcal{O}_j)}{dt} = \alpha_j(1 - \mathcal{O}_j) - \beta_j\mathcal{O}_j, \quad j = 1, \ldots n_c$$

where each Markov chain has two states, closed and open, and the open probability is represented by $\mathcal{O}_j$. α and β are voltage dependent transition rates given by Varghese and Boland (2002) as

$$\alpha = \alpha_0 \exp\left(\frac{z_a V}{V_\tau}\right) \quad \beta = \beta_0 \exp\left(-\frac{z_b V}{V_\tau}\right). \tag{12}$$

Here z_a and z_b are the charges associated with the transition energy barrier located asymmetrically in the electric field of the membrane. For activation gates, $z_{a,m}, z_{b,m} > 0$ and for inactivation gates, $z_{a,h}, z_{b,h} < 0$. Usually we observe that some of these Markov chains have similar dynamics ($\alpha_i = \alpha_j$, and $\beta_i = \beta_j$ for some i, j), and as a consequence, we end up with a model comparable with Hodkin-Huxley models, with the two types of ion-channel gates, activation and inactivation gates respectively.

In fact, in whole-cell recordings several ion channels are measured together and what we observe is an average behaviour of these channels. For this reason, there is no need to consider stochasticity in such models. Therefore, using $\tau_y = 1/(\alpha + \beta)$ as time constant function in the Hodgkin-Huxley equation, both formalisms become equivalent, although with different interpretations (one in terms of gating activation and Markov chains in terms of open probability). Wilson and Callaway (2000) give further details on this approach.

The third kind of expression used are for calcium gated channels that have a significant role in the control of pacemaking activity. Via the coupling of intracellular calcium ion concentration with membrane potential, these group of channels regulates the firing frequency of the spike train (Xia et al. 1998; Drion et al. 2011). Calcium gating of ion-channels is best represented by a Hill expression,

$$\mathcal{O}(Ca_i) = \frac{Ca_i^n}{Ca_i^n + K_{0.5}^n} \tag{13}$$

with Hill-coefficient n and dissociation constant $K_{0.5}$.

2.3.2 Pumps and exchangers

Membrane ATP-ases and cation exchangers function towards balancing the ionic concentrations that are altered by the function of ion-channels. At the membrane of *SNc* pacemaking neurons, plasma membrane calcium ATP-ases (PMCA) and sodium-calcium exchangers (NaCax) move Ca^{2+} ions out from the neuron. Together with this, sodium-potassium ATP-ases (NaK) work towards establishing a steady concentration of Na^+ and K^+ ions.

NaCax form a low affinity - high capacity system (Sedova and Blatter 1999) and their fast response to increase intracellular Ca^{2+} makes them significant in the early stages of Ca^{2+} accumulation. Considering a fast process of exchange, the quantitative description of DiFrancesco and Noble (1985) was used to describe the ionic flux through NaCax (see Appendix A.5).

On the contrary, PMCA is a high affinity - low capacity system and is important in regulating small deviations of Ca^{2+} concentration from its control levels. Additionally, this protein is functionally coupled to the calcium signalling protein calmodulin (CaM) which reversibly binds and activates PMCA in a calcium dependent manner (Osbornm et al. 2004). The Kyoto model (Matsuoka et al. 2007) which describes PMCA activity in cardiac myocytes, with reasonable mechanistic details was adopted assuming the pump characteristics to be conserved between cell types. Figure 2 shows the different mechanistic steps and equations of the model can be seen in Appendix A.6. The description for ion fluxes through NaK is also adopted from the Kyoto model (Matsuoka et al. 2007; Francis et al. 2012a), which describes the dynamics of the different functional states of the protein in a cardiac pacemaker. Once again, conservation of functional characteristics across cell types is assumed. This model assigns the voltage

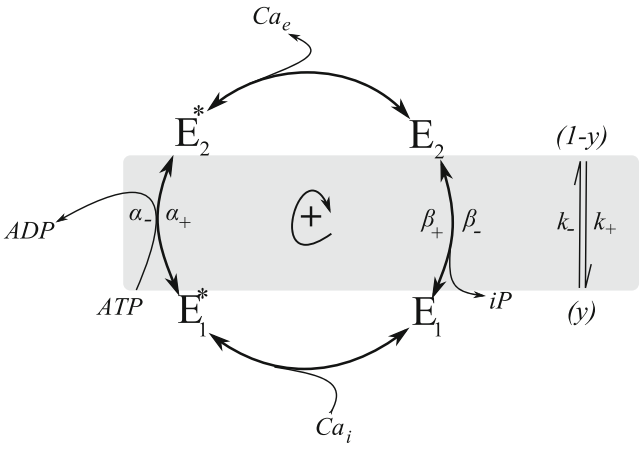

Fig. 2 PMCA transport scheme based on the Kyoto model (Matsuoka et al. 2007): this is a four-state illustration of the transport mechanism of PMCA, which is further reduced to a two-state model by assuming fast binding of calcium ions States E_1 and E_2 correspond to the two different conformation of the protein. Ca^{2+} binds to E_1 in a calmodulin dependent manner to form the intermediate state E_1^*. The conformational change of E_1^* to E_2^* is coupled with an ATP hydrolysis. The protein reverts to its original conformation with the release of Ca^{2+} in the extra-cellular side following the release of the inorganic phosphate

dependence of the pump to the step at which the first sodium ion is released to the outside (see Fig. 3), according to observations made by Rakowski et al. (1997) and the ATP dependence to the step in which protein changes conformation (see model in Appendix A.7).

2.4 Intracellular Ca^{2+} buffering

Intracellular Ca^{2+} levels are critical for the functional state of *SNc* neurons. Apart from its role in the neuron's electrophysiology, Ca^{2+} also have a major part in coordinating various metabolic pathways as a signalling entity. This assignment makes it essential for any cell to keep their levels regulated and calcium buffering mechanisms undertakes this crucial metabolic activity. Calcium binding proteins, including calbindin and calmodulin, are considered to be mobile buffers of calcium and are often clustered near Ca^{2+} hotspots, enabling rapid buffering. On the other hand fixed Ca^{2+} buffers are organelles that sequester Ca^{2+} including the endoplasmic reticulum and mitochondria or proteins anchored to the cytoskeleton and membrane (Verkhratsky and Toescu 1998, Ch. 1).

A precise description of Ca^{2+} dynamics including the transport of Ca^{2+} across ER and mitochondria is not included in this work. Our model does include buffering activity based on the mobile buffers and we have used two of the Ca^{2+} binding proteins that are significant in *SNc* neurons. Calmodulin as a secondary messenger have a regulatory role in membrane excitation. Calbindin, a fast Ca^{2+} buffer, is observed to have significant preventive role in PD pathogenesis (Yamada et al. 1990).

The dynamics of binding of calcium to calbindin is modelled using mass action kinetics based on the high affinity binding kinetics adopted from Nagerl et al. (2000). The

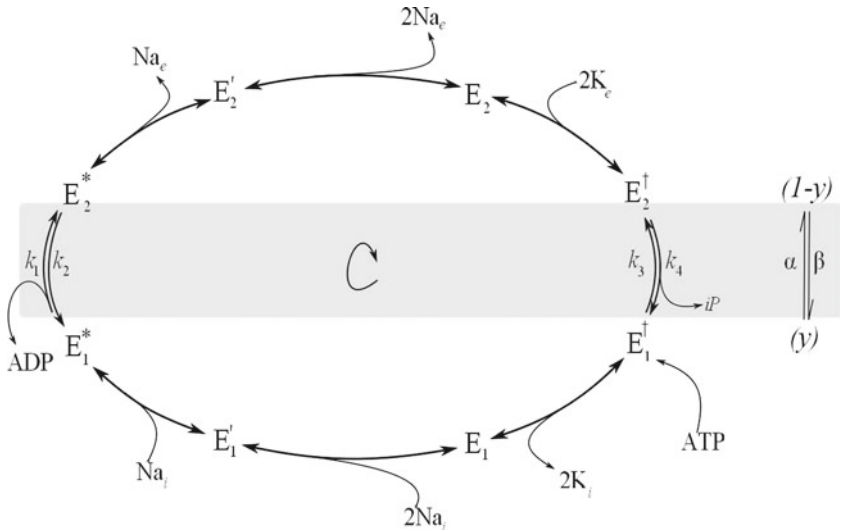

Fig. 3 NaK transport scheme based on the Kyoto model (Matsuoka et al. 2007): the sodium pump exists in two conformational states characterized by differences in their interactions with the ions and ATP. Sodium and ATP bind with very high affinity to the E_1 conformation. Equilibrium binding of two sodium ions facilitates the electrogenic binding of the third sodium ion. The phosphorylation of the enzyme in this bound state leads to a conformational change, which renders the sodium ions open to the external space. Unbinding and release of sodium ions leads to the binding of potassium ions on to the E_2 conformation. This then leads to the dephosphorylation of the enzyme and a conformational change. The equilibrium binding of the ATP molecule to this structure promotes the release of the potassium ions and completes the cycle

dynamics of calmodulin - calcium binding are described using a four state Markov scheme (Francis et al. 2012a) based on Tadross et al. (2008). Models of calbindin and calmodulin dynamics can be seen in Appendices A.8 and A.9, respectively.

2.5 Energy estimation

As discussed before, the distribution of ions across the membrane, to maintain a functional state involves proteins that use energy to transport ions against their gradient. The ATP-ase activity is directly coupled to ATP hydrolysis. The exchangers on the other hand employ the gradient of one ion to transport another ion against their gradient. This activity has an indirect use of energy as ATP, for example with the transport of one Ca^{2+} by NaCax, three Na^{+} ions get transported into the cell, which later is pumped back by NaK.

The energy-transduction associated with membrane excitation may be quantified according to the concepts laid down by Attwell and Laughlin (2001). Within the framework of the model, we can represent the energy expenditure as the amount of ATP required to generate the pump currents (Francis et al. 2012a), as

$$\frac{d(ATP_{\text{use}})}{dt} = \frac{[I_{\text{nak}} + I_{\text{pmca}}]}{F \forall_{cyt}} \tag{14}$$

3 Model simulations and calibration

The pacemaking neuron model was developed as a system of ordinary differential equations (ODEs), simulated in CellML (Miller et al. 2010) and calibrated in MATLAB (2010). The state variables of the system describes the concentrations of different molecular species engaged with the activity across the neuronal membrane, as well as probabilities of different participating protein transporters to be in a conductive state. The design parameters involved in the model may be broadly classified into two groups: (a) the parameters defining the model geometry and (b) coefficients and physical constants from the literature and estimated from experiments for *SNc* in Puopolo et al. (2007). Design parameters corresponding to the adopted geometry of the PMU are provided in Table 2. Table 3 provides other parameters and physical constants obtained from literature implied in the model.

As previously noted, we wanted to gather as much information as possible from the literature, to keep the number of parameters to be estimated to the minimum and therefore, avoid identifiability problems. In addition, we wanted to estimate only those parameters that change substantially from cell to cell, using experimental data from the same neuron. While conductivities of ion channels, pumps and exchangers, as well as buffer concentration (which are all a function of the level of expression of the corresponding proteins), vary from cell to cell, we expect these proteins to have similar functional dynamics in the different cells they are expressed. Therefore, we searched in literature for parameters related to buffer dynamics (Table 3) and pump and exchanger dynamics (see Appendix A.5–A.7). Regarding the ion channels gating dynamics, we fitted those ion channels specially relevant in *SNc* neurons and for which there was experimental data in Puopolo et al. (2007), i.e. cobalt sensitive Ca^{2+} channel and TTX-sensitive Na^{+} channel, and we took the rest from the literature. A collection of all ion channel dynamics can be seen in Table 4.

In the work of Puopolo et al. (2007), experimental currents of Ca^{2+} and Na^{+} were measured from acutely dissociated dopaminergic neurons of *SNc* , capable of spontaneous pacemaking. These currents are the difference currents determined by a voltage clamp protocol in the presence and absence of the respective channel blockers. Note that these measured currents (see Fig. 5 of Puopolo et al. (2007)) are always negative, which implies a persistent inward flow of Ca^{2+} and Na^{+} respectively. From the perspective of dynamical systems, a biochemical arrangement exhibiting spontaneous oscillations involve stable limit cycles. For this to be realized, the sum of net current in a cycle should be zero. Since the data has only negative currents, we may well assume that data do not include the contribution of pumps and exchangers.

In the final fitting, model tuning parameters were estimated from the data for command voltage, that was previously used for generating the current characteristics (Table 5). These parameters include conductance parameters for channels and transporters on the membrane and concentrations of buffer proteins in the cytosol. They are a reflection of the density of different transport proteins and are bound to change according to the choice of design parameters, to match the expected behaviour of the system. Finally, the model was validated by blocking different ion channels and confirming that the model resembles the expected behaviour in a *SNc* neuron.

To optimise the parameters of the model that best fits the data, a global optimization algorithm, SSm GO Egea et al. (2009) was put to use. This algorithm combines a population based meta-heuristic method with a local optimization. As cost functions, we used a sum of common least square functionals with proper weight coefficients to force better solution in those experiments with less uncertainty (Walter and Pronzato 1997). Parameter bounds were based on physiological grounds. Design of the cost function was a complex procedure as the modeling study was limited in available data and the weight coefficients often evolved with the selected objectives. Often

Table 3 Physical and chemical constants and parameters from the literature

Item	Symbol	Value (Units)	Reference
Physical and chemical constants			
Faraday's Constant	F	96485.31 (C/mol)	
Gas Constant	R	8314.472 (J/Kmol.K)	
Calcium valency	z_{Ca}	2	
Sodium valency	z_{Na}	1	
Potassium valency	z_{K}	1	
Common constants in literature			
Extracellular calcium	Ca_e	1.8 (mM)	Puopolo et al. (2007)
Extracellular sodium	Na_e	137 (mM)	Puopolo et al. (2007)
Extracellular potassium	K_e	5.4 (mM)	Puopolo et al. (2007)
Specific membrane capacitance	C_{sp}	0.9 (μF/cm^2)	Gentet et al. (2000)
Cytosolic calcium diffusivity	$\mathcal{D}_{\mathrm{Ca}}$	5.3×10^{-6} (cm^2/s)	Donahue and Abercrombie (1987)
NaCax			
Energy barrier parameter	δ_{xm}	0.35	DiFrancesco and Noble (1985)
Denominator factor	$\mathcal{D}_{\mathrm{xm}}$	0.001	DiFrancesco and Noble (1985)
NaK			
Reaction rates	$k_{2,\mathrm{nk}}$	0.04 (ms^{-1})	Matsuoka et al. (2007)
	$k_{3,\mathrm{nk}}$	0.01 (ms^{-1})	Matsuoka et al. (2007)
	$k_{4,\mathrm{nk}}$	0.165 (ms^{-1})	Matsuoka et al. (2007)
Dissociation constants	$K_{\mathrm{nk,nai}}$	4.05 (mM)	Matsuoka et al. (2007)
	$K_{\mathrm{nk,nae}}$	69.8 (mM)	Matsuoka et al. (2007)
	$K_{\mathrm{nk,ki}}$	32.88 (mM)	Matsuoka et al. (2007)
	$K_{\mathrm{nk,ke}}$	0.258 (mM)	Matsuoka et al. (2007)
PMCA			
Reaction rates	$k_{2,\mathrm{pc}}$	0.001 (ms^{-1})	Matsuoka et al. (2007)
	$k_{3,\mathrm{pc}}$	0.001 (ms^{-1})	Matsuoka et al. (2007)
	$k_{4,\mathrm{pc}}$	1 (ms^{-1})	Matsuoka et al. (2007)
Dissociation constants	$K_{\mathrm{pc,e}}$	2 (mM)	Matsuoka et al. (2007)
Buffer Dynamics			
Calbindin reaction rates	$k_{\mathrm{calb,b}}$	10000 (1/mM.s)	Nagerl et al. (2000)
	$k_{\mathrm{calb,d}}$	2 (1/s)	Nagerl et al. (2000)
Calmodulin reaction rates	$k_{\mathrm{cam}}^{\mathrm{cb}}$	1.2×10^7 (1/mM^2.s)	Tadross et al. (2008)
	$k_{\mathrm{cam}}^{\mathrm{cd}}$	3 (1/s)	Tadross et al. (2008)
	$k_{\mathrm{cam}}^{\mathrm{nb}}$	3.7×10^9 (1/mM^2.s)	Tadross et al. (2008)
	$k_{\mathrm{cam}}^{\mathrm{nd}}$	3000 (1/s)	Tadross et al. (2008)
Other design parameters			
Body temperature	T	37 (°C)	
Cytosolic ATP	$[ATP]$	2 (mM)	

the parameter search space had to be modified to have a balance between selected criteria and speed of optimization, however in most instances they were kept in a range that was physiologically justified. As an exception, we had to particularly extend the allowed range of variation in the intra-cellular calcium concentration, such that the model reproduced the electrical activity with enough detail. For instance, restricting the allowed variations of intra-cellular calcium in a range observed experimentally by Wilson and Callaway (2000) (50-250 nM) kept us from a good solution. It was required to raise the upper bound of calcium concentration to 1000 nM for an acceptable solution. The physiological interpretation of this is discussed with the results.

As discussed previously, for the remaining channels, the parameters for their dynamic gating were adapted from literature (Table 4). Although this is not the optimum routine for identifying various channel parameters for the model, for

Table 4 Gating dynamics of the different channel used in the model

Channel	$\mathcal{O}_c$	Source
Ca^{2+} channel, L type	$\mathcal{O}_{\mathrm{ca,l}} = m_{\mathrm{ca,l}} h_{\mathrm{ca,l}}$	fitted, based on Amini et al. (1999)
	$\frac{d(m_{\mathrm{ca,l}})}{dt} = \frac{1/\left(1+\exp\left(\frac{V+15}{-7}\right)\right) - m_{\mathrm{ca,l}}}{7.68 \cdot \exp\left(-\left[\frac{V+65}{17.33}\right]^2\right) + 0.723}$	
	$h_{\mathrm{ca,l}} = \frac{0.00045}{0.00045 + Ca_i}$	
Na^+ channel	$\mathcal{O}_{\mathrm{na}} = m_{\mathrm{na}}^3 h_{\mathrm{na}}$	fitted from Puopolo et al. (2007)
	$\frac{d(m_{\mathrm{na}})}{dt} = 1.965 \exp\left(\frac{1.7127V}{V_\tau}\right)(1-m_{\mathrm{na}})$	
	$-0.0424 \exp\left(\frac{-1.5581V}{V_\tau}\right) m_{\mathrm{na}}$	
	$\frac{d(h_{\mathrm{na}})}{dt} = 0.0001 \exp\left(\frac{-2.4317V}{V_\tau}\right)(1-h_{\mathrm{na}})$	
	$-0.5296 \exp\left(\frac{1.1868V}{V_\tau}\right) h_{\mathrm{na}}$	
K^+ channel, SK-type	$\mathcal{O}_{\mathrm{k,sk}} = \frac{Ca_i^{4.2}}{Ca_i^{4.2} + 0.00035^{4.2}}$	Xia et al. (1998)
K^+ delayed rectifier	$\mathcal{O}_{\mathrm{k,dr}} = m_{\mathrm{k,dr}}^3$	Amini et al. (1999)
	$\frac{d(m_{\mathrm{k,dr}})}{dt} = \frac{1/\left(1+\exp\left(\frac{V+25}{-12}\right)\right) - m_{\mathrm{k,dr}}}{\frac{18}{\left(1+\exp\left(\frac{V+39}{8}\right)\right)} + 1}$	
K^+ channel, internal rectifier	$\mathcal{O}_{\mathrm{k,ir}} = 1/\left(1+\exp\left(\frac{V+85}{12}\right)\right)$	Chan et al. (2007)
HCN channel	$\frac{d(\mathcal{O}_{\mathrm{hcn}})}{dt} = k_{\mathrm{f,hcn}} \mathcal{O}_{\mathrm{hcn}} - k_{\mathrm{r,hcn}}(1-\mathcal{O}_{\mathrm{hcn}})$	Francis et al. (2012a)
	$k_{\mathrm{f,hcn}} = k_{\mathrm{f,free}} \mathcal{P}(C) + k_{\mathrm{f,bnd}}(1-\mathcal{P}(C))$	
	$k_{\mathrm{r,hcn}} = k_{\mathrm{r,free}} \mathcal{P}(O) + k_{\mathrm{r,bnd}}(1-\mathcal{P}(O))$	
	$\mathcal{P}(C) = 1/\left[1+\frac{cAMP}{0.001163}\right] \mathcal{P}(O) = 1/\left[1+\frac{cAMP}{0.00145}\right]$	
	$k_{\mathrm{f,free}} = \frac{0.006}{1+\exp\left(\frac{V+87.7}{6.45}\right)}$ $k_{\mathrm{r,free}} = \frac{0.08}{1+\exp\left(-\frac{V+51.7}{7}\right)}$	
	$k_{\mathrm{f,bnd}} = \frac{0.0268}{1+\exp\left(\frac{V+94.2}{13.3}\right)}$ $k_{\mathrm{r,bnd}} = \frac{0.08}{1+\exp\left(-\frac{V+35.5}{7}\right)}$	

Table 5 Estimated parameters

Item	Symbol	Value (Units)
Conductances		
L-type Ca^{2+} channel	$g_{ca,l}$	2101.2 (nS)
Na^+ channel	g_{na}	907.68 (nS)
SK-type K^+ channel	$g_{k,sk}$	2.2515 (nS)
K^+ delayed rectifier	$\mathcal{G}_{k,dr}$	31.237 (n℧)
K^+ inward rectifier	$\mathcal{G}_{k,ir}$	13.816 (n℧)
HCN channel	g_{nahcn}	51.1 (nS)
Na^+ leak	$g_{na,leak}$	0.0053 (nS)
NaCax	k_{xm}	0.0166 (pA.ms)
NaK	k_{nak}	1085.7 (pA.ms)
PMCA	k_{pmca}	2.233 (pA.ms)
Buffering		
Total cytosolic calmodulin	Cam_{total}	0.0235 (mM)
Total cytosolic calbindin	$Calb_{total}$	0.005 (mM)

the reason discussed before, limitation in the data selected to develop the model forces this measure to avoid identifiability issues.

4 Results

A model for *SNc* pacemaking was developed based on the recordings of Puopolo et al. (2007) on acutely dissociated neurons. The model includes a representative sodium channel that is sensitive to TTX. Ca^{2+} ions enter through L-type calcium channel and expelled by means of a sodium-calcium exchanger (NaCax) and a calcium pump (PMCA). T-type calcium channels were not included in the final model as the contribution from them to the calcium current with our data fits, using a gating dynamics from Amini et al. (1999), was found to be insignificant. The dynamics of K^+ transport are controlled by three potassium channels, the delayed rectifier and internal rectifier being voltage controlled and the SK-type being calcium concentration controlled. The levels of Na^+ and K^+ are kept in check by the action of the sodium-potassium pump (NaK). We have considered only transport of Na^+ through the cAMP-dependent HCN channels as their range of activity is closer to the Nernst potential of K^+ ions and we do not expect significant flow of K^+ ions through this channel.

4.1 Dynamic behaviour

The model was calibrated for obtaining normal pacemaking exhibit by *SNc* neurons. In order to assess the validity of the model, it was calibrated for obtaining behaviour expected of these neurons with respect to two different channel blockers. The presence of Tetradotoxin (TTX), a sodium channel blocker have been reported to block the spiking currents and the neuron is expected to demonstrate slow oscillations driven by calcium currents (Amini et al. 1999; Ibanez-Sandoval et al. 2007). Also, the presence of L-type calcium channel blockers like dihydropyridines is reported to abolish the pacemaking activity, but may be reinstated with an increase in cytosolic cAMP levels (Chan et al. 2007). These observations are experimented in the mathematical model by setting the corresponding channel conductance to zero.

Figure 4 shows the model simulation profiles generated using the estimated parameters and the experimental data used for the calibration: (a) using pacemaking voltage that was later used as command voltage in the experiment of Puopolo et al. (2007) for analysing the Na^+ and Ca^{2+} currents, (b) TTX sensitive Na^+ ion channel currents and (c) cobalt sensitive Ca^{2+} ion channel currents. These figures show the performance of the different estimations, where we note the correct match of the spiking frequency, as well as the main features of the spiking save for voltage, Na^+ channel current and Ca^{2+} channel current.

In the model, as we are using the differential form of the voltage expression, and as discussed before, we can eliminate problems with respect to drift in computed variables if charge is conserved in the system (Hund et al. 2001). For a condition of stable oscillations, the system should exhibit stable limit cycle in the corresponding variables. In our model, we see that intracellular cationic species (Ca^{2+}, Na^+ and K^+) exhibit such limit cycles (Figs. 4d, e and f).

One apparent discrepancy that our model has with experimental observation (Wilson and Callaway 2000) is with respect to maximal calcium concentration. One limitation of our model is that it only captures the dynamics of events occurring in the vicinity of the membrane and is not reflective of the average behaviour in the cytosol. The experiments, on the other hand, are an optical recording of fluorescence that gives an average behaviour over the cross-section. Closer to the membrane, various cellular components work together to form a region that allows high concentration of calcium but limits its diffusion into the bulk of the cytoplasm (Parekh 2008). Such calcium hotspots, generally referred to as the micro-domain exists between the cell membrane and endoplasmic reticulum as well as between mitochondria and endoplasmic reticulum, farther from the membrane. The higher calcium concentration observed with our model is rather reflective of calcium concentrations that can exist in such a micro-domain and optical measurements gives the average concentrations across the neuronal cross-section. A detailed picture of variations in calcium concentrations along the cross-section would necessitate the extension of this model into multiple compartments.

What we have in our model is only sodium conductances that are sensitive to TTX. The deactivation of sodium

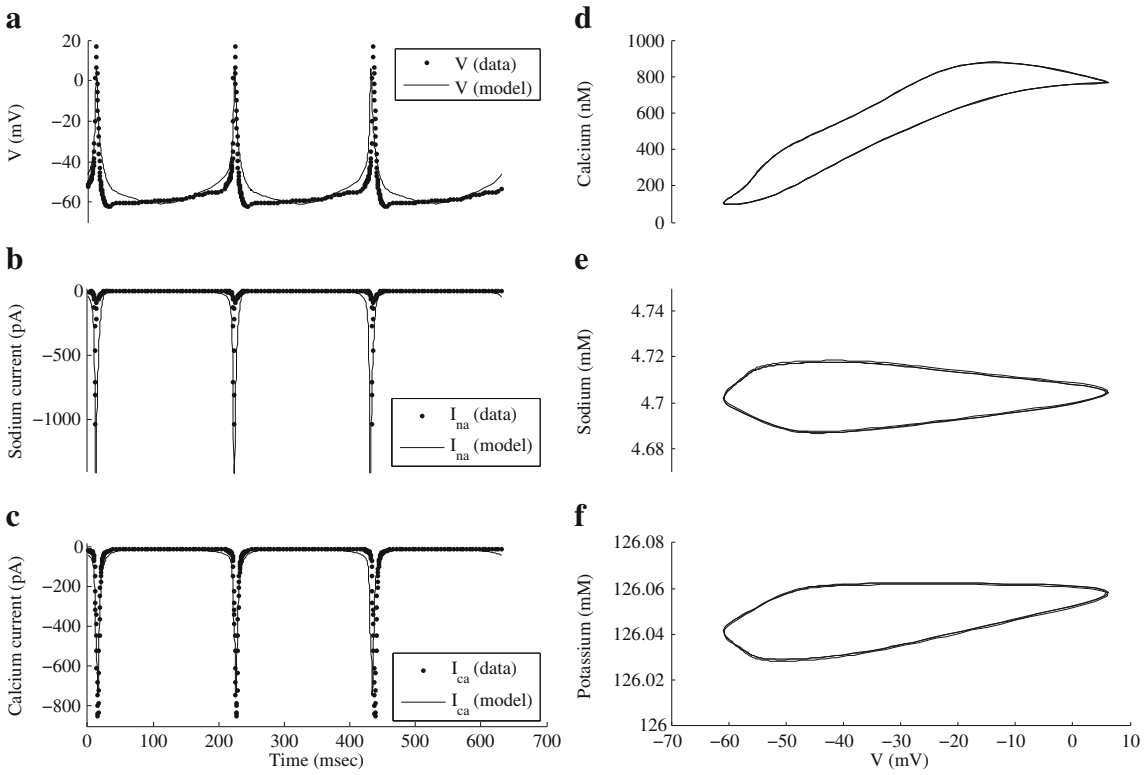

Fig. 4 The response of the model with the estimated parameters. The tuning parameters of the model was fit from data on pacemaking in dissociated neurons by Puopolo et al. (2007) including the spontaneous spikes in its membrane potential (**a**), TTX sensitive sodium currents (**b**) and cobalt sensitive calcium currents. The model shows stable limit cycles in the concentration of the cations involved (**d, e, f**)

channels by TTX need not necessarily be equally effective on all subtypes of sodium channels (Goldin 1999; Du et al. 2009). There are reports on neuron to neuron variability for the extent of block in *SNc* neurons (Puopolo et al. 2007). Studies involving blocking sodium conductance with TTX have shown a cessation of the spontaneous activity (Choi et al. 2003) and in many other cases a very slow oscillatory behaviour was observed. This rhythm set by a pacemaker-like slow depolarisation has been termed as the slow oscillatory potential (SOP) (Amini et al. 1999). On these grounds, sodium channels that are not blocked by TTX are in all probability contributing to SOPs.

Repetitive slow depolarizations were observed when the TTX block study was carried out in an NMDA bath (Ibanez-Sandoval et al. 2007). Since NMDA is applied to mimic glutamate input, for the neuronal soma this would be equivalent of receiving dendritic inputs as Na^+ ions. For this reason, a partial revival of sodium channel conductance from the blocked condition should lead to slow depolarizations. To analyse this our model was simulated by initially completely blocking the TTX sensitive Na^+ current and later partially enhancing this particular conductance. Figures 5, 6 and 7 shows the model behaviour when the sodium channels are inhibited in the presence of TTX. By blocking sodium channels with TTX, regular spikes are replaced by SOPs with oscillations of similar frequency. However, the SOPs are not sustained for long. Later with a partial revival of sodium channels, slow and repetitive oscillations of membrane potential is observed. The time course of this slow wave is comparable to the slow depolarizations observed in the experiments of Ibanez-Sandoval et al. (2007). This slow depolarization is calcium dependent and may be abolished by blocking the calcium currents (results not shown) and should not be confused with the SOP.

These profiles supports the observations made from some of the previous modelling studies on these neurons (Amini et al. 1999; Wilson and Callaway 2000; Kuznetsova et al. 2010; Drion et al. 2011) and justifies the selection of ion-channels. Although the currents through the sodium channels (I_{na}) and potassium delayed rectifier ($I_{k,dr}$) contribute to visible spikes, the underlying rhythm for both SOPs and slow depolarization, seem to be set by the concerted effort of currents through calcium channels ($I_{ca,l}$) with the potassium SK-type channel ($I_{k,sk}$) and internal rectifier ($I_{k,ir}$), with ample support from membrane pumps and exchangers.

Of particular interest is the dynamics of cation pumps during the TTX block (Fig. 6) which was not clearly evident in earlier models (Amini et al. 1999) which employed

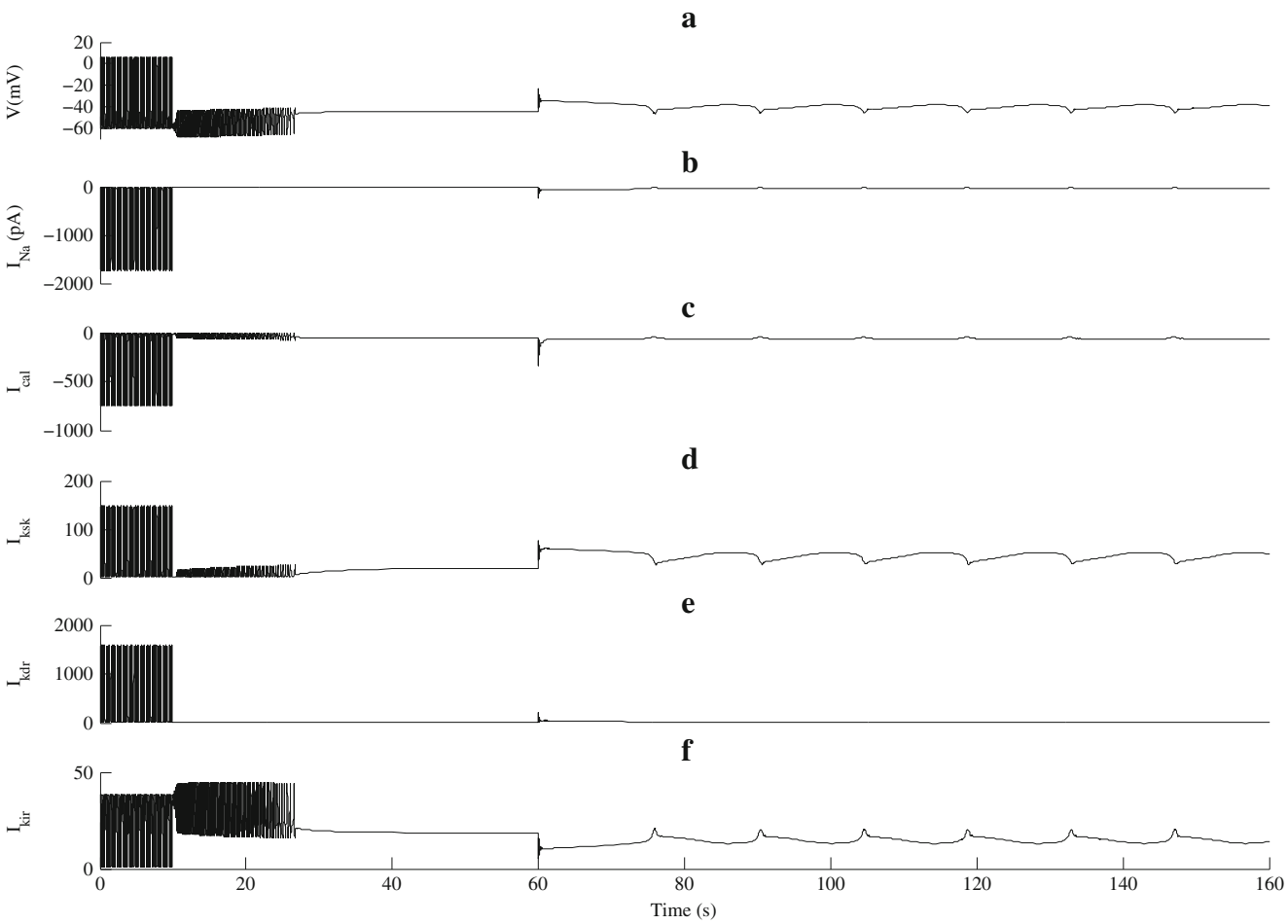

Fig. 5 Blocking fast sodium channels by TTX brings forth the system that underlies the spontaneous pacemaking activity of *SNc* neurons (**a**) The TTX block was simulated by reducing the sodium channel conductance to zero at 10 s, the sodium currents were partially recovered from 60 s to simulate a partial block by TTX. The spiking wave is replaced by SOPs with the application of TTX which eventually dies down. Slow depolarizing waves are generated when sodium channels are partially replaced. **b**, **e** The currents responsible for spiking activity, the fast sodium and delayed rectifier potassium currents are silenced with the TTX block (**c**) The calcium channels have an important role in sustaining the oscillations. These channels are ably supported by the potassium channels **d**, **f**

a simple Michaelis-Menten type expression for the pump's action or models that did not use them at all (Wilson and Callaway 2000; Kuznetsova et al. 2010). This experiment testifies to the role of calcium ions in initiation of pacemaking and the significance of membrane pumps and exchangers in establishing the background oscillations that underlie pacemaking.

The blockade of L-type calcium channel currents ($I_{ca,l}$) by dihydropyridines (DHP) is achieved by setting the channel conductance ($g_{ca,l}$) to zero, in the model. DHP block keeps the system from spontaneous oscillations, and the pacemaking reappears with an increase in the levels of cyclic adenosine monophosphate (cAMP) in the cytosol (Fig. 8). This is in accordance with the observation made by Chan et al. (2007) on mouse neurons. According to their theory, the blockade of L-type calcium channels brings about a drop in cytosolic Ca^{2+} levels, which in turn lifts the restriction imposed on the calcium-inhibited isoforms of the enzymes adenylyl cyclase. These enzymes catalyse the production of cAMP from ATP molecules at the membrane under the influence of G proteins as a part of the G protein signalling cascade. With reduced concentration of Ca^{2+} in the cytosol, an increase in cAMP would shift the voltage dependence of HCN channels that are allosterically regulated by these signalling molecules. This shift in voltage dependence re-establishes pacemaking, however with the help of Na^{+} ions.

The proposed model effectively links the energy allocation for ion concentration maintenance of *SNc* neurons with its pacemaker firing by means of the activity of ion-exchange proteins at the neuronal membrane. As discussed above, the switch from a calcium driven pacemaking

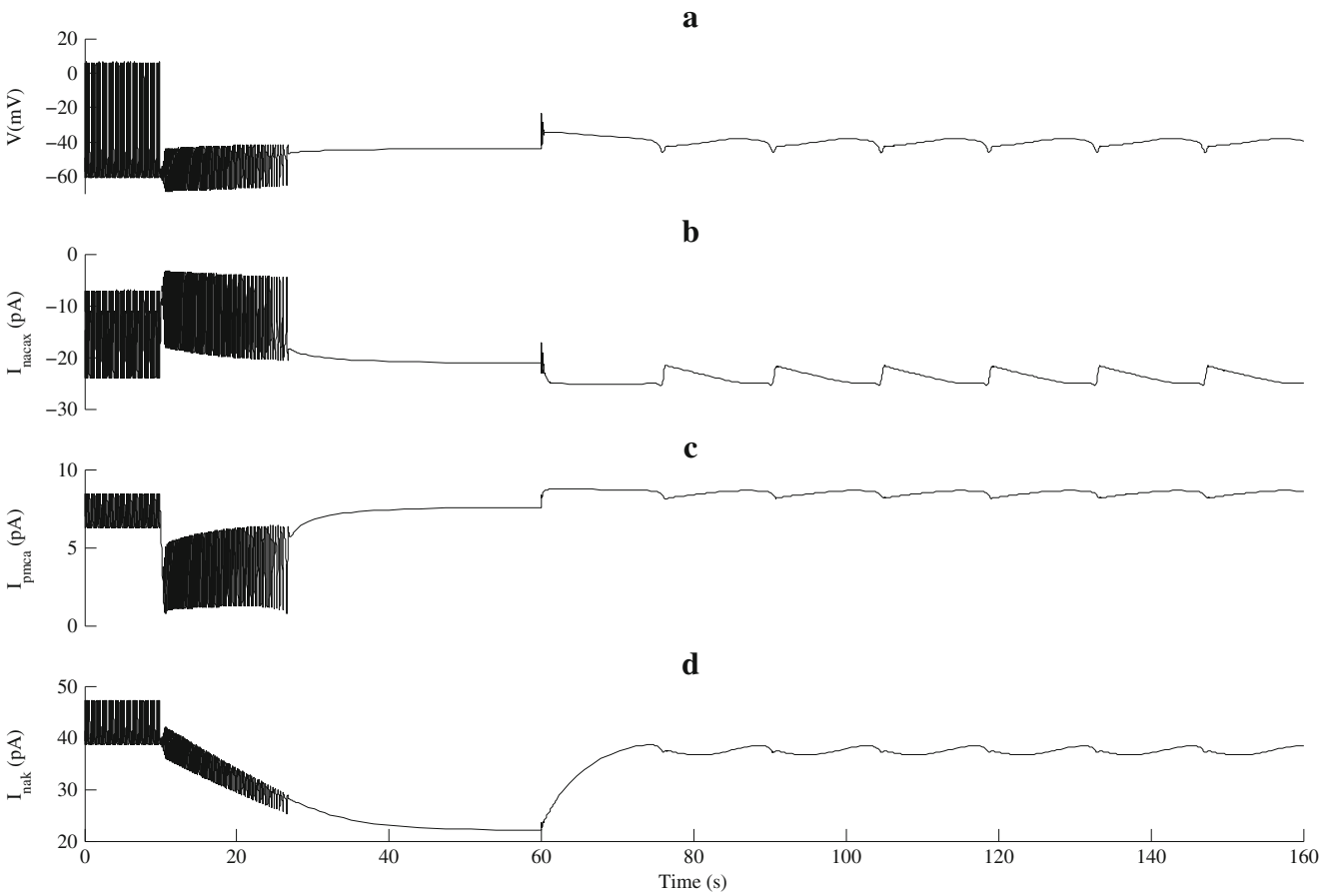

Fig. 6 Contribution of membrane transporters observed with the block of fast sodium channels by TTX. The TTX block was simulated as described in Fig. 5. The sodium-calcium exchanger have a significant role in initiation of the oscillations, and the two pumps seems to be contributing towards maintaining the ionic levels

mode to a sodium driven mode should effectively reduce the energy load on these neurons owing to the prevailing concentration gradients of these ions. Also, neuronal excitability is strongly dependent on cytosolic calcium levels with higher cytosolic calcium leading to lower excitability. This dependence is mostly due to calcium dependent steps in the membrane electrophysiology that have larger response time. When the mode of pacemaking switches to the sodium-driven mode, there is a significant reduction in the intracellular Ca^{2+} levels (Fig. 8f). This in turn makes the cell excitable and we see an increased spiking rate. Despite the increased firing rates, we see that the ATP use at the membrane per spike is considerably less (Figs. 8e, 9). The ATP use per second observed by this study is however higher and may be a limit of such modelling studies. This aspect is discussed later.

4.2 Energy implications of calcium channel block

In the analysis, we consider scenarios that have been experimentally observed Chan et al. (2007). We look at the difference in energy use by *SNc* neurons in two distinct conditions. In the first scenario, we consider the normal operating mode of this neuron in which they undergo spontaneous oscillations driven by Ca^{2+} ions. In the second case, the Ca^{2+} ions are blocked by means of a L-type calcium channel blocker and with the help of an enhanced level of the signalling molecule cAMP, oscillations are recovered, but driven by Na^{+} ions.

Figure 9 brings shows noticeable differences in the energy use by these neurons in the given experimental situations. There is an apparent reduction in energy consumption by these neurons and the use of energy appears to decrease with the extend of channel blocking achieved. Even with a higher frequency of oscillation, the use of energy is significantly less with the calcium block (About 60 % less per spike).

One of the leading thoughts in the field of therapeutic intervention of PD pathogenesis is to target mechanisms that impart stress on the dopaminergic neurons. Some of the observations made on calcium channels suggest a potential for subjecting these neurons to L-type calcium channel

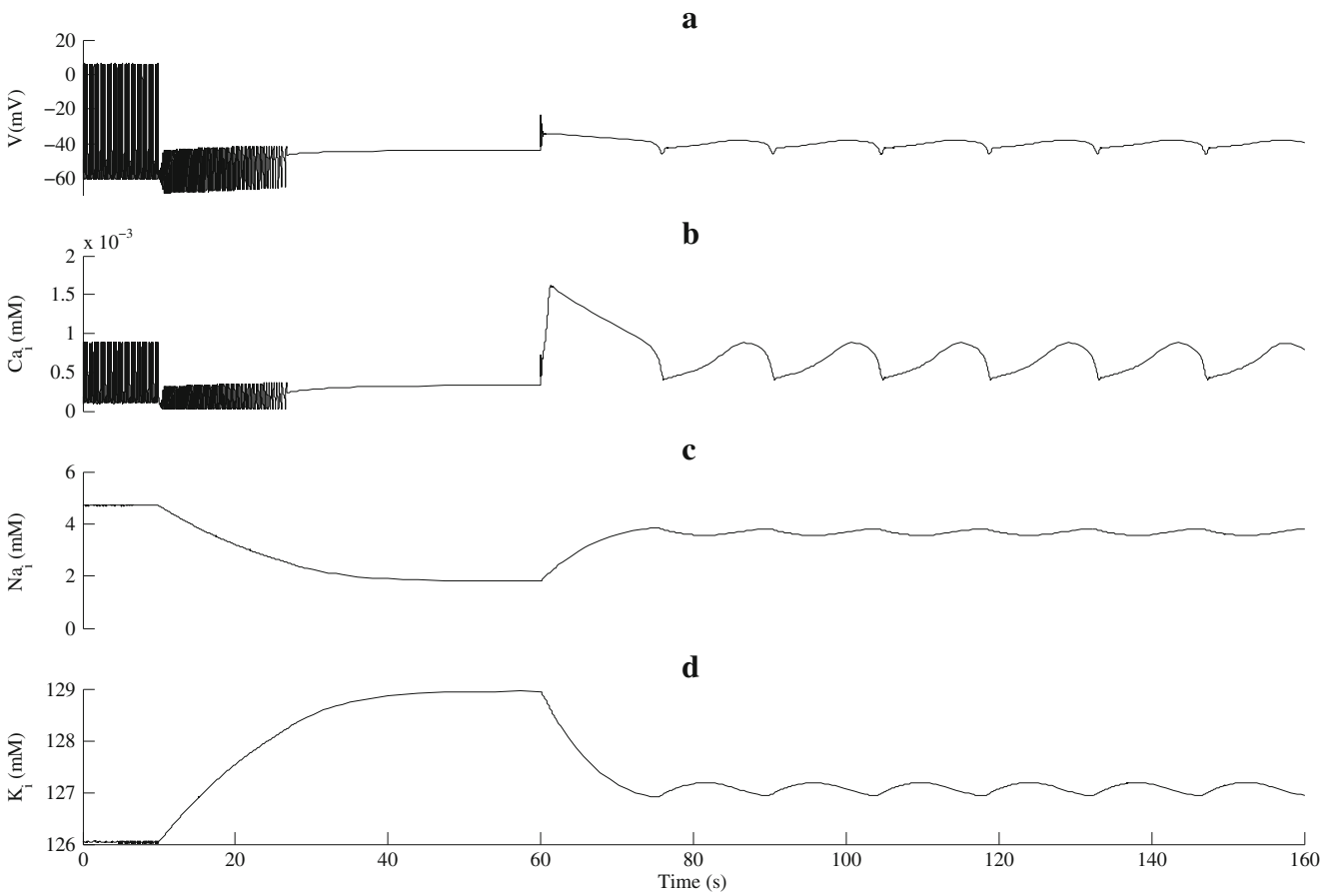

Fig. 7 Oscillations in intracellular cation concentrations with the block of fast sodium channels by TTX. The TTX block was simulated as described in Fig. 5. Simulations suggests the oscillations to be driven by a concerted action of calcium and potassium ions. The SOPs are mostly driven by oscillations in calcium where as potassium ions have an equally important role during the slow depolarizing wave

blockers and thereby reduce the overall stress. In this work, we have attempted to build a mathematical framework that explicitly incorporates the dynamics of the ionic species involved. The significance of this approach is in its ability to predict energy utilization by the system. This framework can be readily extended to a larger model which includes detailed energy metabolism.

4.3 Stability of the limit cycle

One of the defining aspect of *SNc* pacemaking is its spontaneous spiking and such self-sustained oscillations imply the existence of a stable limit cycle. Any perturbation on the model from the equilibrium must then, make the system return to this limit cycle. For a complex model that we have at hand, a visual depiction of this process is not an easy task. Instead, we numerically find the 'monodromy matrix' of the local linearisation of a cycle and the eigenvalues of this matrix are employed to predict the stability and convergence of the limit cycle Viswanath (2001).

A brief description of the monodromy matrix method is given in Appendix B. The spectral properties of the monodromy matrix can also provide information regarding the components of the system. For a periodic system close to a stable limit cycle (such as a simple periodic orbit), the trajectories in state space should converge to the limit cycle. This analysis is only guaranteed to be valid for small deviations from the limit cycle, but is a useful numerical technique for studying local stability. In addition, for a stable limit cycle, the largest eigenvalue is generically unity, and the magnitude of the second largest eigenvalue gives an estimate of the rate of convergence to the cycle.

From this numerical analysis we observe that for our proposed model with the estimated parameters, the oscillations converge to a stable limit cycle (see Fig. 6a). In our model, the largest eigenvalue is indeed at 1. However, the second largest eigenvalues is very close to one, which suggests that the rate of convergence to the limit cycle would be very slow. The normalised magnitude of the eigenvector corresponding to the second largest eigenvalue

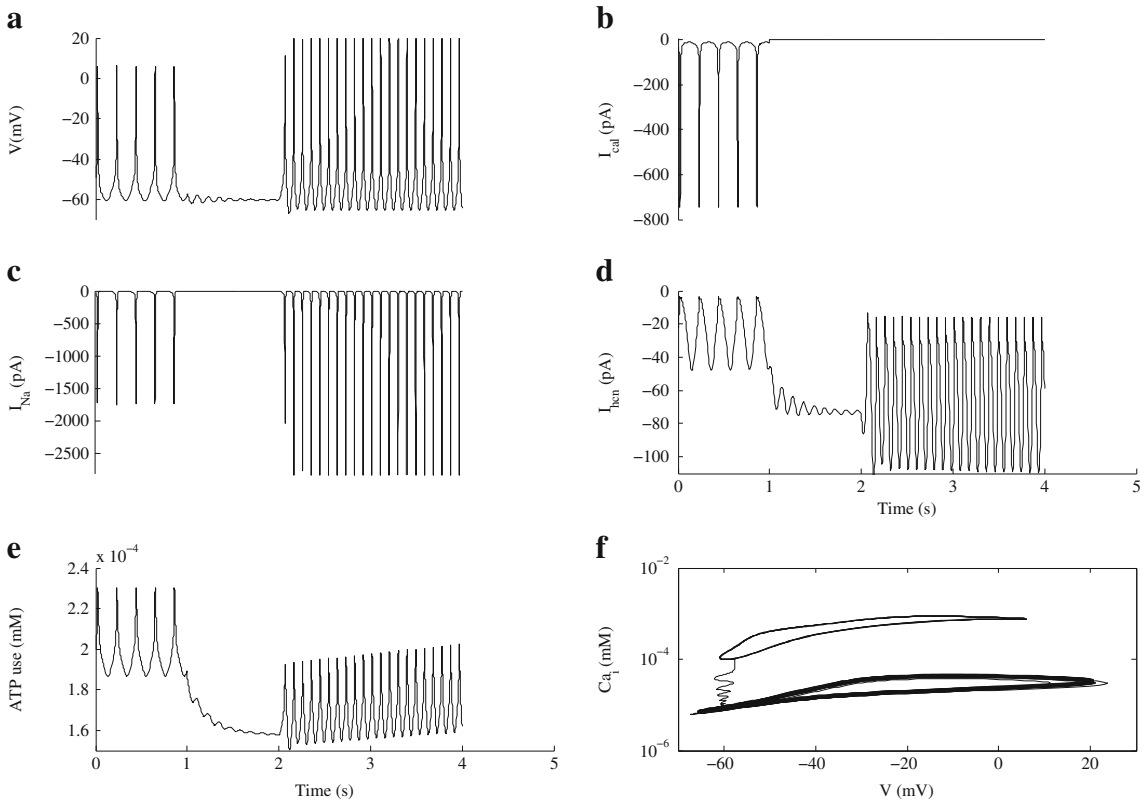

Fig. 8 Regular spiking experienced without L-type calcium channel at higher cAMP concentrations. **a** The spontaneous pacemaking at the *SNc* membrane ceases with the introduction of L-type calcium channel blocker at 1000 ms. In the simulations this is achieved by setting the L-type calcium channel conductance to zero. The pacemaking is re-established by an increase in cAMP concentration from 2000 ms. **b** The L type calcium currents completely ceases with the block, however T type calcium channels are more active owing to a membrane that is more hyperpolarized. **c** There is higher sodium influx through sodium channels and the HCN channels (**d**). The HCN channels are activated by both hyperpolarization and increased cAMP levels. **e** The cell consumes less energy as ATP per spike however, at an increased spiking rate. **f** There is stable limit cycles in calcium levels in both cases, with the L-type channel blocked calcium levels are reduced by an order of magnitude

(see Fig. 6b) suggests the variables contributing to the slow dynamics involve components that correspond to the calcium dynamics, including the buffers, and the HCN channel (Table 6).

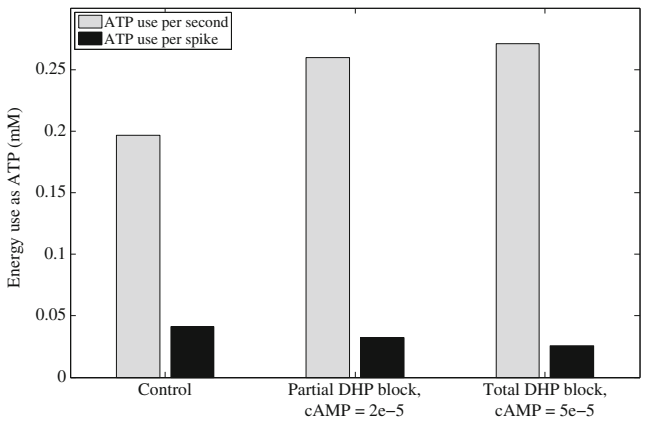

Fig. 9 ATP use with respect to the two modes of pacemaking

4.4 Energy implications

All biochemical events of a living system involve energy. Having a central role in determining the dynamical behaviour of the system, energy flow and storage often seals the fate of the system. Ion transport is an integral part of this feature and for an excitatory cells like neurons, this becomes a defining feature. Regular spiking, extensive arborisation together with bursting on stimulation makes the *SNc* neuron very tight on its energy budget and any constraint on its energy pathways can have long term consequences on the neurons' existence.

Our model also aims to understand the energy use by *SNc* neurons, based on its varied mechanisms of ion conduction that results in its characteristic pacemaking activity. Energy is used up by the cellular machinery, primarily to maintain the levels of cations across the membrane. Among the various factors that influence ATP consumption, the most important is the difference in cation concentrations from their control levels. Also, the density of cation pumps on the

Table 6 Limit Cycle stability

(a) Leading eigenvalues of monodromy MATRIX (estimated via numerical simulation)	
i	$\|\lambda_i\|$
1	1
2	0.9868
3	0.9377
4	0.9258
5	0.4273
6	0.1101
(b) Properties from the second largest eigenvalue	
State	Normalised eigenvector corresponding to the second largest eigenvalue
V	8.7e-7
Ca_i	-255.56
Na_i	-0.0005
K_i	$-1.93e-6$
Cam	42.608
$Calb$	88.4
m_{na}	0.0005
h_{na}	0.0072
$\mathcal{O}_{\text{hcn}}$	3.183
m_{cal}	0.0034
m_{kdr}	-0.0004
$\mathcal{O}_{\text{nk}}$	-0.0004
$\mathcal{O}_{\text{pc}}$	$-1.153e-5$

membrane is significant, being the site of action. Changes in the level of Ca^{2+} ions would have significant impact on energy use, as the concentration difference is orders of magnitude higher compared to other cations.

To understand the impact of Ca^{2+} ions on energy utilization during membrane oscillation, ATP consumption patterns were compared with the case when pacemaking was driven by Na^+ ions. According to the observations of Chan et al. (2007), juvenile *SNc* neurons in an animal model oscillate in a Na^+ dependent manner with the help of HCN channels. The half-activation voltage of these channels in this model progressively hyperpolarize owing to reduction in cAMP levels and an increase in the expression of L-type calcium channels. Based on this observation we simulate a L-type calcium channel block and substitute its electrophysiological role with HCN channels, by means of altering their voltage dependence with an increase in cAMP concentration. An increase in cAMP revives the pacemaking in *SNc* neurons, however the spikes are less hyperpolarized and faster (Fig. 8). Corresponding observations on the energy consumption pattern are depicted in Fig. 9. With the given model, a change of pacemaking from a Ca^{2+} driven mode to a Na^+ driven mode, has an impact on the energy use at the membrane. Although the apparent energy use seem to be higher, ATP required per spike of the oscillation is less compared to the control. If the cells adapts its conductances to reach the optimum firing rate, the energy use at the membrane should hence be lower than the control case.

5 Discussion

A characteristic of life is its innate ability of self-regulation. Life forms take immediate control of what happens within them with the help of molecules that help communicate between the various sub-components that make up their cells. Calcium with its unique chemistry found a specific role in the evolution of life (Jaiswal 2001). Ca^{2+} ions serve as a diffusible second messenger and find themselves at the crux of diverse physiological activities including ion-transport, signal transduction, transcription control, energy metabolism etc. Neurons remarkably use Ca^{2+} to modulate its electrical activity at fast time scales using calcium dependent ion channels and at slow time scales with the help of buffers and other intracellular signal cascades.

Calcium has an intricate relationship with the other important secondary messenger involved in energy metabolism, cAMP. In addition to the activation of enzyme adenylyl cyclase that would increase cAMP, increased levels of Ca^{2+} can also enhance the activity of enzyme phosphodiesterase, which breaks down cAMP, by means of calcium-calmodulin complexes. Conversely, an increase in cAMP level can increase Ca^{2+} influx through L-type calcium channels via protein kinase A activation (Nicholls et al. 2001). Since in the specific experiments we are looking at, as these channels are blocked, this feedback element of cAMP-Ca^{2+} crosstalk is removed. This ensures an increase in cytosolic cAMP to levels that would shift the activation voltage of HCN channels to a range that would restore pacemaking.

We see that the increase in cAMP concentration to revive pacemaking increases with the extent of the blockade on the L-type calcium channels. Further, the use of energy as ATP per spike is reduced with the increasing blockade of L-type channels. This correlates with the reduction in Ca^{2+} ion influx, as the cells now do not require to pump as much ions of Ca^{2+} as before, per cycle of pacemaking. However, the ATP use per second of pacemaking activity is higher compared to the control because of an increase in the pacemaking rate. This is one limitation with the modelling as it does not completely reflect experimental data that shows a return to pacemaking at a frequency only slightly higher than that without blockade.

It is important to note that in the experiments on L-type channel blocks, the restoration of pacemaking happens after around an hour. Also the firing rate of these neurons after the restored activity is reasonably near to the control firing rates. A lower influx of Ca^{2+} would imply

lower levels of calcium-calmodulin complex which in turn would have consequences on protein expression levels. As proteins on the membranes are also constantly recycled as a part of cell maintenance, a change in expression levels would be reflected in the conductance values of at least a few of the membrane ion-transporters. These differences would be reflected in the firing rate of these neurons. Future developments of the model presented here would include adaptation of the channel conductances as a result changes in calcium-calmodulin.

Not withstanding these limitations, in its current form, our model suggests the follow possible effects of L-type channel blockers. (i) The energy usage per spike is expected to decrease. Therefore, unless there is a significant increase in spike rate, we expect lower energy consumption; (ii) The average and peak Ca^{2+} load in the cytosol is reduced. Both of these effects are consistent with reduced neuronal stress and thereby improved longevity.

Acknowledgments F.F, M.R.G. and R.H.M. acknowledge support by Science Foundation Ireland grant 07/IN.1/I1838.

Appendix A: Model equations

A.1 Ion dynamics

$$\frac{d(Ca_i)}{dt} = J_{\mathrm{m,Ca}} - (J_{\mathrm{calb}} + 4J_{\mathrm{cam}}) \tag{15}$$

$$\frac{d(Na_i)}{dt} = J_{\mathrm{m,Na}} \tag{16}$$

$$\frac{d(K_i)}{dt} = J_{\mathrm{m,K}} \tag{17}$$

A.2 Membrane ion fluxes

$$J_{\mathrm{m,Ca}} = \frac{1}{z_{\mathrm{Ca}} F \mathcal{V}_{cyt}} (I_{\mathrm{Ca}} + 2I_{\mathrm{pmca}} - 2I_{\mathrm{nacax}}) \tag{18}$$

$$J_{\mathrm{m,Na}} = \frac{1}{z_{\mathrm{Na}} F \mathcal{V}_{cyt}} (3I_{\mathrm{nak}} + 3I_{\mathrm{nacax}} + I_{\mathrm{Na}}) \tag{19}$$

$$J_{\mathrm{m,K}} = \frac{1}{z_{\mathrm{K}} F \mathcal{V}_{cyt}} (I_K - 2I_{\mathrm{nak}}) \tag{20}$$

A.3 Membrane potential

$$\frac{d(V)}{dt} = \frac{F \mathcal{V}_{cyt}}{C_{\mathrm{sp}} \mathcal{A}_{\mathrm{pmu}}} [\frac{d(Na_i)}{dt} + 2\frac{d(Ca_i)}{dt} + \frac{d(K_i)}{dt}] \tag{21}$$

A.4 Membrane ion-channel currents

$$I_{\mathrm{Ca}} = \left(\sum_x g_{\mathrm{ca,x}} \mathcal{O}_{\mathrm{ca,x}} \right) \sqrt{Ca_e Ca_i} \frac{\sinh\left(\frac{V - \bar{V}_{\mathrm{Ca}}}{V_\tau}\right)}{\mathrm{sinhc}\left(\frac{V}{V_\tau}\right)} \tag{22}$$

$$I_{\mathrm{K}} = \left(\sum_x g_{\mathrm{k,x}} \mathcal{O}_{\mathrm{k,x}} \right) \sqrt{K_e K_i} \frac{\sinh\left(\frac{V - \bar{V}_{\mathrm{K}}}{2V_\tau}\right)}{\mathrm{sinhc}\left(\frac{V}{2V_\tau}\right)} + \left(\sum_y g_{\mathrm{k,y}} \mathcal{O}_{\mathrm{k,y}} \right) (V - \bar{V}_{\mathrm{K}}) \tag{23}$$

$$I_{\mathrm{Na}} = \left(\sum_x g_{\mathrm{na,x}} \mathcal{O}_{\mathrm{na,x}} \right) \sqrt{Na_e Na_i} \frac{\sinh\left(\frac{V - \bar{V}_{\mathrm{Na}}}{2V_\tau}\right)}{\mathrm{sinhc}\left(\frac{V}{2V_\tau}\right)} \tag{24}$$

Here, x includes all channels modelled by the GHK equation and y the set of all channels modelled by the linear conductance relationship.

A.5 Plasma membrane sodium calcium exchanger (NaCax)

$$I_{\mathrm{nacax}} = k_{\mathrm{xm}} \frac{Na_i^3 Ca_e \cdot e^{\left(\frac{\delta_{\mathrm{xm}} V}{V_\tau}\right)} - Na_e^3 Ca_i \cdot e^{\left(\frac{(\delta_{\mathrm{xm}}-1) V}{V_\tau}\right)}}{(1 + \mathcal{D}_{\mathrm{xm}}[Na_i^3 Ca_e + Na_e^3 Ca_i]) \left(1 + \frac{Ca_i}{0.0069}\right)} \tag{25}$$

A.6 Plasma membrane calcium ATPase (PMCA)

$$I_{\mathrm{pmca}} = K_{\mathrm{pc}} [k_{1,\mathrm{pc}} \mathcal{P}(E^*_{1,\mathrm{pc}}) y_{\mathrm{pc}} - k_{2,\mathrm{pc}} \mathcal{P}(E^*_{2,\mathrm{pc}})(1 - y_{\mathrm{pc}})] \tag{26}$$

$$\frac{d(y_{\mathrm{pc}})}{dt} = \beta_{\mathrm{pc}}(1 - y_{\mathrm{pc}}) - \alpha_{\mathrm{pc}} y_{\mathrm{pc}}$$

$$\beta_{\mathrm{pc}} = k_{2,\mathrm{pc}} \mathcal{P}(E^*_{2,\mathrm{pc}}) + k_{4,\mathrm{pc}} \mathcal{P}(E_{2,\mathrm{pc}})$$

$$\alpha_{\mathrm{pc}} = k_{1,\mathrm{pc}} \mathcal{P}(E^*_{1,\mathrm{pc}}) + k_{3,\mathrm{pc}} \mathcal{P}(E_{1,\mathrm{pc}})$$

$$\mathcal{P}(E^*_{1,\mathrm{pc}}) = \left[1 + \frac{K_{\mathrm{pc,i}}}{Ca_i}\right]^{-1} \quad \mathcal{P}(E_{1,\mathrm{pc}}) = 1 - \mathcal{P}(E^*_{1,\mathrm{pc}})$$

$$\mathcal{P}(E^*_{2,\mathrm{pc}}) = \left[1 + \frac{K_{\mathrm{pc,e}}}{Ca_e}\right]^{-1} \quad \mathcal{P}(E_{2,\mathrm{pc}}) = 1 - \mathcal{P}(E^*_{2,\mathrm{pc}})$$

$$k_{1,\mathrm{pc}} = \frac{1}{1 + 0.1/[ATP]}$$

$$K_{\mathrm{pc,i}} = \left[\frac{180 - 6.4}{1 + \frac{CaCam}{0.000,05}} + 6.4\right] \times 10^{-5}$$

$$K_{\mathrm{pc}} = \kappa_{\mathrm{pmca}} \left[\frac{10.56 \times CaCam}{CaCam + 0.000,05} + 1.2\right]$$

A.7 Plasma membrane sodium-potassium ATPase (NaK)

$$I_{\mathrm{nk}} = K_{\mathrm{nk}}[k_{1,\mathrm{nk}}\mathcal{P}(E^*_{1,\mathrm{nk}})y_{\mathrm{nk}} - k_{2,\mathrm{nk}}\mathcal{P}(E^*_{2,\mathrm{nk}})(1-y_{\mathrm{nk}})] \quad (27)$$

$$\begin{aligned}
\frac{d(y_{\mathrm{nk}})}{dt} &= \beta_{\mathrm{nk}}(1-y_{\mathrm{nk}}) - \alpha_{\mathrm{nk}}y_{\mathrm{nk}} \\
\beta_{\mathrm{nk}} &= k_{2,\mathrm{nk}}\mathcal{P}(E^*_{2,\mathrm{nk}}) + k_{4,\mathrm{nk}}\mathcal{P}(E^\dagger_{2,\mathrm{nk}}) \\
\alpha_{\mathrm{nk}} &= k_{1,\mathrm{nk}}\mathcal{P}(E^*_{1,\mathrm{nk}}) + k_{3,\mathrm{nk}}\mathcal{P}(E^\dagger_{1,\mathrm{nk}}) \\
\mathcal{P}(E^*_{1,\mathrm{nk}}) &= \left[1 + \frac{K_{\mathrm{nk,nai}}}{Na_i}\left(1 + \frac{K_i}{K_{\mathrm{nk,ki}}}\right)\right]^{-1} \\
\mathcal{P}(E^\dagger_{1,\mathrm{nk}}) &= \left[1 + \frac{K_{\mathrm{nk,ki}}}{K_i}\left(1 + \frac{Na_i}{K_{\mathrm{nk,nai}}}\right)\right]^{-1} \\
\mathcal{P}(E^*_{2,\mathrm{nk}}) &= \left[1 + \frac{K_{\mathrm{nk,nae}}}{Na_{\mathrm{eff}}}\left(1 + \frac{K_e}{K_{\mathrm{nk,ke}}}\right)\right]^{-1} \\
\mathcal{P}(E^\dagger_{2,\mathrm{nk}}) &= \left[1 + \frac{K_{\mathrm{nk,ke}}}{K_e}\left(1 + \frac{Na_{\mathrm{eff}}}{K_{\mathrm{nk,nae}}}\right)\right]^{-1} \\
Na_{\mathrm{eff}} &= Na_e e^{-0.82V/V_\tau} \\
k_{1,\mathrm{nk}} &= \frac{0.37}{1 + 0.094/[ATP]}
\end{aligned}$$

A.8 Ca^{2+} Buffering by calbindin

$$\begin{aligned}
J_{\mathrm{calb}} &= k_{\mathrm{calb,b}} \cdot Ca_i \cdot Calb - k_{\mathrm{calb,d}} \cdot CaCalb \quad (28) \\
Calb_{\mathrm{total}} &= Calb + CaCalb \\
\frac{d(Calb)}{dt} &= -J_{\mathrm{calb}}
\end{aligned}$$

A.9 Ca^{2+} Buffering by calmodulin

$$\begin{aligned}
J_{\mathrm{cam}} &= \alpha_{\mathrm{cam}} \cdot Cam - \beta_{\mathrm{cam}} \cdot CaCam \quad (29) \\
Cam_{\mathrm{total}} &= Cam + CaCam \\
\frac{d(Cam)}{dt} &= -J_{\mathrm{cam}} \\
\alpha_{\mathrm{cam}} &= K^{\mathrm{cb}}_{\mathrm{cam}}K^{\mathrm{nb}}_{\mathrm{cam}}\left[\frac{1}{K^{\mathrm{cb}}_{\mathrm{cam}} + k^{\mathrm{nd}}_{\mathrm{cam}}} + \frac{1}{k^{\mathrm{cd}}_{\mathrm{cam}} + K^{\mathrm{nb}}_{\mathrm{cam}}}\right] \\
\beta_{\mathrm{cam}} &= k^{\mathrm{cd}}_{\mathrm{cam}}k^{\mathrm{nd}}_{\mathrm{cam}}\left[\frac{1}{K^{\mathrm{cb}}_{\mathrm{cam}} + k^{\mathrm{nd}}_{\mathrm{cam}}} + \frac{1}{k^{\mathrm{cd}}_{\mathrm{cam}} + K^{\mathrm{nb}}_{\mathrm{cam}}}\right] \\
K^{\mathrm{cb}}_{\mathrm{cam}} &= k^{\mathrm{cb}}_{\mathrm{cam}}Ca_i^2 \\
K^{\mathrm{nb}}_{\mathrm{cam}} &= k^{\mathrm{nb}}_{\mathrm{cam}}Ca_i^2
\end{aligned}$$

Appendix B: Monodromy matrix method

A system of one dimensional equations given by

$$\dot{x} = f(x,\varphi), \quad x \in \mathbb{R}^n, \quad \varphi \in \mathbb{R}^p. \quad (30)$$

where x and φ are the respective vectors for the variables and parameters, is considered to have a periodic solution if the solution is a closed trajectory, i.e., $x(t+T) = x(t)$ for all real t. The smallest value of $T(T > 0)$, for which this holds is called the 'period'. If $\phi_t(x_0)$ denote the solution of Eq. (30) at time t starting from x_0 at time $t = 0$, then the Monodromy matrix is defined as,

$$M = \left.\frac{\partial \phi_T(x)}{\partial x}\right|_{x=x_0} \quad (31)$$

and may be obtained as the solution of the variation equation at time T. The variation equation is obtained by perturbing the system in the neighbourhood of a point ϕ^* on the periodic solution $\phi(t)$ of the system. Upon linearisation we have, $\dot{y}(t) = A(t) \cdot y$, where $A(t)$ is the Jacobian of f around $x(t)$. If $Y(t)$ is the fundamental solution of this linear equation with $Y(0) = I$,

$$\frac{d(Y(t))}{dt} = \left.\frac{\partial f(x)}{\partial x}\right|_{x(t)} \cdot Y(t), \quad Y(0) = I, \quad (32)$$

then $M = Y(T)$.

References

Alberts, B., Johnson, A., Lewis, J., Raff, M., Roberts, K., Walter, P. (2002). *Molecular biology of the cell* (pp. 1227–1242). New York: Garland Science.

Amini, B., Clark, J.W. Jr, Canavier, C.C. (1999). Calcium dynamics underlying pacemaker-like and burst firing oscillations in midbrain dopaminergic neurons: a computational study. *Journal of Neurophysiology*, *82*(5), 2249–2261.

Attwell, D., & Laughlin, S.B. (2001). An energy budget for signaling in the grey matter of the brain. *Journal of Cerebral Blood Flow & Metabolism*, *21*, 1133–1145.

Balsa-Canto, E., Banga, J.R., García, M.R. (2010). Dynamic model building using optimal identification strategies, with applications in bioprocess engineering. In *Process systems engineering: Dynamic process modeling* (Vol. 7, pp. 441–467). Weinheim: Wiley-VCH Verlag GmbH & Co. KGaA.

Canavier, C. (1999). Sodium dynamics underlying burst firing and putative mechanisms for the regulation of the firing pattern in midbrain dopamine neurons: a computational approach. *Journal of Computational Neuroscience*, *6*, 49–69.

Canavier, C.C., & Landry, R.S. (2006). An increase in ampa and a decrease in sk conductance increase burst firing by different mechanisms in a model of a dopamine neuron *in vivo*. *Journal of Neurophysiology*, *96*(5), 2549–2563.

Chan, C.S., Guzman, J.N., Guzman, J.N., Ilijic, E., Mercer, J.N., Rick, C., Tkatch, T., Meredith, G.E., Surmeier, D.J. (2007). 'Rejuvenation' protects neurons in mouse models of parkinson's disease. *Nature*, *447*, 1081–1086.

Choi, Y.M., Kim, S.H., Uhm, D.Y., Park, M.K. (2003). Glutamate-mediated [ca2+] c dynamics in spontaneously firing dopamine neurons of the rat substantia nigra pars compacta. *Journal of cell science*, *116*(13), 2665–2675.

Cloutier, M., & Wellstead, P. (2010). The control systems structures of energy metabolism. *Journal of The Royal Society Interface*, *7*(45), 651–665.

Da Cunha, C., Wietzikoski, S., Wietzikoski, E.C., Miyoshi, E., Ferro, M.M., Anselmo-Franci, J.A., Canteras, N.S. (2003). Evidence for the substantia nigra pars compacta as an essential component of a memory system independent of the hippocampal memory system. *Neurobiology of Learning and Memory*, *79*(3), 236–242.

Damier, P., Hirsch, E.C., Agid, Y., Graybiel, A.M. (1999). The substantia nigra of the human brain. II. Patterns of loss of dopamine-containing neurons in parkinson's disease. *Brain*, *122*(Pt 8), 1437–1448.

DiFrancesco, D., & Noble, D. (1985). A model of cardiac electrical activity incorporating ionic pumps and concentration changes. *Philosophical Transactions of the Royal Society B: Biological Sciences*, *307*, 353–398.

Donahue, B.S., & Abercrombie, R.F. (1987). Free diffusion coefficient of ionic calcium in cytoplasm. *Cell Calcium*, *8*(6), 437–448.

Drion, G., Massotte, L., Sepulchre, R., Seutin, V. (2011). How modeling can reconcile apparently discrepant experimental results: The case of pacemaking in dopaminergic neurons. *PLoS Computational Biology*, *7*(5), e1002,050.

Du, Y., Nomura, Y., Liu, Z., Huang, Z.Y., Dong, K. (2009). Functional expression of an arachnid sodium channel reveals residues responsible for tetrodotoxin resistance in invertebrate sodium channels. *Journal of Biological Chemistry*, *284*(49), 33869–33875.

Duchen, M.R., Verkhratsky, A., Muallem, S. (2008). Mitochondria and calcium in health and disease. *Cell Calcium*, *44*(1), 1–5.

Egea, J.A., Balsa-Canto, E., García, M.S.G., Banga, J.R. (2009). Dynamic optimization of nonlinear processes with an enhanced scatter search method. *Industrial & Engineering Chemistry Research*, *48*(9), 4388–4401.

Endresen, L.P., Hall, K., Høye, J.S., Myrheim, J. (2000). A theory for the membrane potential of living cells. *European Biophysics Journal*, *29*(2), 90–103.

Ermentrout, G.B., & Terman, D. (2010). Mathematical foundations of neuroscience. *Interdisciplinary applied mathematics*. New York: Springer.

Francis, F., García, M.R., Middleton, R.H. (2012a). Energetics of ion transport in dopaminergic substantia nigra neurons. In P. Wellstead & M. Cloutier (Eds.), *Systems biology of Parkinson's disease* (pp. 81–109). New York: Springer.

Francis, F., García, M.R., Wellstead, P., Middleton, R. (2012b). L-type calcium channel block and energy implications for substantia nigra neurons. *Movement Disorders*, *27*(1), S205. 16th International Congress of parkinson's disease and movement disorders, Dublin, IRELAND, JUN 17-21, 2012.

Gentet, L.J., Stuart, G.J., Clements, J.D. (2000). Direct measurement of specific membrane capacitance in neurons. *Biophysical Journal*, *79*, 314–320.

Goldin, A.L. (1999). Diversity of mammalian voltage-gated sodium channels. *Annals of the New York Academy of Sciences*, *868*(1), 38–50.

Grace, A.A., & Bunney, B.S. (1983). Intracellular and extracellular electrophysiology of nigral dopaminergic neurons–2. action potential generating mechanisms and morphological correlates. *Neuroscience*, *10*(2), 317–331.

Hainsworth, A.H., Röper, J., Kapoor, R., Ashcroft, F.M. (1991). Identification and electrophysiology of isolated pars compacta neurons from guinea-pig substantia nigra. *Neuroscience*, *43*(1), 81–93.

Hodgkin, A.L., & Huxley, A.F. (1952). A quantitative description of membrane current and its application to conduction and excitation in nerve. *The Journal of Physiology*, *117*(4), 500–544.

Hodgkin, A.L., & Katz, B. (1949). The effect of sodium ions on the electrical activity of the giant axon of the squid. *The Journal of Physiology*, *108*(1), 37–77.

Hund, T.J., Kucera, J.P., Otani, N.F., Rudy, Y. (2001). Ionic charge conservation and long-term steady state in the Luo-Rudy dynamic cell model. *Biophysical Journal*, *81*, 3324–3331.

Ibanez-Sandoval, O., Carrillo-Reid, L., Galarraga, E., Tapia, D., Mendozam, E., Gomora, J.C., Aceves, J., Bargas, J. (2007). Bursting in substantia nigra pars reticulata neurons *in vitro*: possible relevance for parkinson disease. *Journal of Neurophysiology*, *98*(4), 2311–2323.

Iwatsubo, T., Nakano, I., Fukunaga, K., Miyamoto, E. (1991). Ca2+/calmodulin-dependent protein kinase II immunoreactivity in Lewy bodies. *Acta Neuropathol*, *82*, 159–163.

Izhikevich, E.M. (2007). *Dynamical systems in neuroscience: The geometry of excitability and bursting. Computational neuroscience*. Cambridge: MIT Press.

Jaiswal, J.K. (2001). Calcium - how and why? *Journal of Biosciences*, *26*, 357–363.

Komendantov, A.O., Komendantova, O.G., Johnson, S.W., Canavier, C.C. (2004). A modeling study suggests complementary roles for gabaa and nmda receptors and the sk channel in regulating the firing pattern in midbrain dopamine neurons. *Journal of Neurophysiology*, *91*(1), 346–357.

Kuznetsova, A.Y., Huertas, M.A., Kuznetsov, A.S., Paladini, C.A., Canavier, C.C. (2010). Regulation of firing frequency in a computational model of a midbrain dopaminergic neuron. *Journal of Computational Neuroscience*, *28*(3), 389–403.

Lesnick, T.G., Papapetropoulos, S., Mash, D.C., Ffrench-Mullen, J., Shehadeh, L., de Andrade, M., Henley, J.R., Rocca, W.A., Ahlskog, J.E., Maraganore, D.M. (2007). A genomic pathway approach to a complex disease: axon guidance and parkinson disease. *PLoS Genetics*, *3*(6), e98.

Lloyd, C.M., Halstead, M.D.B., Nielsen, P.F. (2004). CellML: its future, present and past. *Progress in biophysics and molecular biology*, *85*(2), 433–450.

Lloyd, C.M., Lawson, J.R., Hunter, P.J., Nielsen, P.F. (2008). The CellML model repository. *Bioinformatics*, *24*(18), 2122–2123.

Matell, M.S., & Meck, W.H. (2000). Neuropsychological mechanisms of interval timing behavior. *Bioessays*, *22*(1), 94–103.

MATLAB (2010). *version 7.10.0 (R2010a)*. The MathWorks Inc.

Matsuda, W., Furuta, T., Nakamura, K.C., Hioki, H., Fujiyama, F., Arai, R. (2009). Single nigrostriatal dopaminergic neurons form widely spread and highly dense axonal arborizations in the neostriatum. *The Journal of Neuroscience*, *29*, 444–453.

Matsuoka, S., Jo, H., Kuzumoto, M., Takeuchi, A., Saito, R., Noma, A. (2007). *Modeling energetics of ion transport, membrane sensing and systems biology of the heart* (pp. 435–455). Weinheim: Wiley-VCH Verlag GmbH & Co. KGaA.

Miller, A.K., Marsh, J., Reeve, A., Garny, A., Britten, R., Halstead, M., Cooper, J., Nickerson, D.P., Nielsen, P.F. (2010). An overview of the CellML API and its implementation. *BMC Bioinformatics*, *11*, 178.

Moran, L., Duke, D., Deprez, M., Dexter, D., Pearce, R., Graeber, M. (2006). Whole genome expression profiling of the medial and lateral substantia nigra in parkinson's disease. *Neurogenetics*, *7*, 1–11.

Nagerl, U.V., Novo, D., Mody, I., Vergara, J.L. (2000). Binding kinetics of calbindin-D-28k determined by flash photolysis of caged Ca2+. *Biophysical Journal*, *79*, 3009–3018.

Nedergaard, S., Flatman, J., Engberg, I. (1993). Nifedipine-and omega-conotoxin-sensitive ca2+ conductances in guinea-pig substantia nigra pars compacta neurones. *The Journal of Physiology*, *466*(1), 727–747.

Nicholls, J.G., Martin, A.R., Wallace, B.G., Fuchs, P.A. (2001). *From neuron to brain*. Sinauer Associates Sunderland, MA.

Osbornm, K.D., Zaidi, A., Mandal, A., Urbauer, R.J., Johnson, C.K. (2004). Single-molecule dynamics of the calcium-dependent

activation of plasma-membrane Ca2+-ATPase by calmodulin. *Biophysical Journal*, *87*, 1892–1899.

Parekh, A.B. (2008). Ca2+ microdomains near plasma membrane Ca2+ channels: impact on cell function. *The Journal of Physiology*, *586*(13), 3043–3054.

Poignard, C., Silve, A., Campion, F., Mir, L.M., Saut, O., Schwartz, L. (2011). Ion fluxes, transmembrane potential, and osmotic stabilization: a new dynamic electrophysiological model for eukaryotic cells. *European Biophysics Journal*, *40*, 235–246.

Puopolo, M., Raviola, E., Bean, B.P. (2007). Roles of Subthreshold Calcium Current and Sodium Current in Spontaneous Firing of Mouse Midbrain Dopamine Neurons. *The Journal of Neuroscience*, *27*(3), 645–656.

Putzier, I., Kullmann, P.H.M., Horn, J.P., Levitan, E.S. (2009). Cav1.3 channel voltage dependence, not ca2+ selectivity, drives pacemaker activity and amplifies bursts in nigral dopamine neurons. *The Journal of Neuroscience*, *29*, 15414–15419.

Rakowski, R.F., Gadsby, D.C., De Weer, P. (1997). Voltage dependence of the Na/K pump. *Journal of Membrane Biology*, *155*, 105–112.

Sedova, M., & Blatter, L.A. (1999). Dynamic regulation of $[Ca^{2+}]_i$ by plasma membrane Ca(2+)-ATPase and Na^+/Ca^{2+} exchange during capacitative Ca^{2+} entry in bovine vascular endothelial cells. *Cell Calcium*, *25*, 333–343.

Surmeier, D.J. (2007). Calcium, ageing, and neuronal vulnerability in parkinson's disease. *The Lancet Neurology*, *6*(10), 933–938.

Surmeier, D.J., Mercer, J.N., Chan, C.S. (2005). Autonomous pacemakers in the basal ganglia: who needs excitatory synapses anyway *Current opinion in neurobiology*, *15*(3), 312–318.

Tadross, M.R., Dick, I.E., Yue, D.T. (2008). Mechanism of local and global Ca2+ sensing by calmodulin in complex with a Ca2+ channel. *Cell*, *133*, 1228–1240.

Takada, M., Kang, Y., Imanishi, M. (2001). Immunohistochemical localization of voltage-gated calcium channels in substantia nigra dopamine neurons. *European Journal of Neuroscience*, *13*(4), 757–762.

Tepper, J.M. (2010). Neurophysiology of substantia nigra dopamine neurons: Modulation by gaba. In H. Steiner & K. Tseng (Eds.), *Handbook of basal ganglia structure and function, handbook of behavioral neuroscience*. Elsevier: Academic Press.

Varghese, A., & Boland, L.M. (2002). Computing transient gating charge movement of voltage-dependent ion channels. *Journal of Computational Neuroscience*, *12*(2), 123–137.

Verkhratsky, A., & Toescu, E.C. (1998). *Integrative aspects of calcium signalling*. New York: Springer.

Viswanath, D. (2001). The lindstedt–poincar technique as an algorithm for computing periodic orbits. *SIAM Review*, *43*(3), 478–495.

Walter, E., & Pronzato, L. (1997). Identification of parametric models from experimental data. *Communications and control engineering series*. Berlin: Springer.

Wellstead, P., & Cloutier, M. (2011). An energy systems approach to Parkinson's disease. *Wiley Interdisciplinary Reviews: Systems Biology and Medicine*, *3*, 1–6.

Wellstead, P., & Cloutier, M. (2012). Modelling and simulation of brain energy metabolism: Energy and parkinson's disease. *Systems biology of parkinson's disease* (pp. 19–38). New York: Springer.

Wilson, C.J., & Callaway, J.C. (2000). Coupled Oscillator Model of the Dopaminergic Neuron of the Substantia Nigra. *Journal of Neurophysiology*, *83*(5), 3084–3100.

Wolfart, J., & Roeper, J. (2002). Selective coupling of t-type calcium channels to sk potassium channels prevents intrinsic bursting in dopaminergic midbrain neurons. *The Journal of Neuroscience*, *22*(9), 3404–3413.

Xia, X.M., Fakler, B., Rivard, A., Wayman, G., Johnson-Pais, T., Keen, J.E., Ishii, T., Hirschberg, B., Bond, C.T., Lutsenko, S., Maylie, J., Adelman, J.P. (1998). Mechanism of calcium gating in small-conductance calcium-activated potassium channels. *Nature*, *395*, 503–507.

Yamada, T., McGeer, P.L., Baimbridge, K.G., McGeer, E.G. (1990). Relative sparing in Parkinson's disease of substantia nigra dopamine neurons containing calbindin-D28K. *Brain Research*, *526*, 303–307.

Zhou, W., Long, C., Fink, A.L., Uversky, V.N. (2010). Calbindin-d 28k acts as a calcium-dependent chaperone suppressing α-synuclein fibrillation *in vitro*. *Central European Journal of Biology*, *5*(1), 11–20.